ESC European Society of Cardiology

Cardiovascular Research (2021) **117**, 2377–2394
doi:10.1093/cvr/cvaa300

Haploinsufficiency of *Tmem43* in cardiac myocytes activates the DNA damage response pathway leading to a late-onset senescence-associated pro-fibrotic cardiomyopathy

Leila Rouhi[1], Sirisha M. Cheedipudi [1], Suet Nee Chen[1†], Siyang Fan[1], Raffaella Lombardi[1‡], Xiaofan Chen[1§], Cristian Coarfa [2], Matthew J. Robertson[2], Priyatansh Gurha[1], and Ali J. Marian [1]*

[1]Center for Cardiovascular Genetics, Institute of Molecular Medicine and Department of Medicine University of Texas Health Sciences Center at Houston, 6770 Bertner Street, Suite C900A, TX 77030, USA; and [2]Department of Molecular and Cellular Biology, Baylor College of Medicine, Houston, TX 77030, USA

Received 21 July 2020; revised 18 September 2020; editorial decision 5 October 2020; accepted 6 October 2020; online publish-ahead-of-print 18 October 2020

Time for primary review: 14 days

Aims Arrhythmogenic cardiomyopathy (ACM) encompasses a genetically heterogeneous group of myocardial diseases whose manifestations are sudden cardiac death, cardiac arrhythmias, heart failure, and in a subset fibro-adipogenic infiltration of the myocardium. Mutations in the *TMEM43* gene, encoding transmembrane protein 43 (TMEM43) are known to cause ACM. The purpose of the study was to gain insights into the molecular pathogenesis of ACM caused by *TMEM43* haploinsufficiency.

Methods and results The *Tmem43* gene was specifically deleted in cardiac myocytes by crossing the *Myh6-Cre* and floxed *Tmem43* mice. *Myh6-Cre:Tmem43*$^{W/F}$ mice showed an age-dependent phenotype characterized by an increased mortality, cardiac dilatation and dysfunction, myocardial fibrosis, adipogenesis, and apoptosis. Sequencing of cardiac myocyte transcripts prior to and after the onset of cardiac phenotype predicted early activation of the TP53 pathway. Increased TP53 activity was associated with increased levels of markers of DNA damage response (DDR), and a subset of senescence-associated secretary phenotype (SASP). Activation of DDR, TP53, SASP, and their selected downstream effectors, including phospho-SMAD2 and phospho-SMAD3 were validated by alternative methods, including immunoblotting. Expression of SASP was associated with epithelial–mesenchymal transition and age-dependent expression of myocardial fibrosis and apoptosis in the *Myh6-Cre:Tmem43*$^{W/F}$ mice.

Conclusion TMEM43 haploinsufficiency is associated with activation of the DDR and the TP53 pathways, which lead to increased expression of SASP and an age-dependent expression of a pro-fibrotic cardiomyopathy. Given that TMEM43 is a nuclear envelope protein and our previous data showing deficiency of another nuclear envelope protein, namely lamin A/C, activates the DDR/TP53 pathway, we surmise that DNA damage is a shared mechanism in the pathogenesis of cardiomyopathies caused by mutations involving nuclear envelope proteins.

* Corresponding author. Tel: +1 713 500 2350, E-mail: ali.j.marian@uth.tmc.edu
† Present address. Division of Cardiology, University of Colorado, Boulder, CO, USA.
‡ Present address. Division of Cardiology, Department of Advanced Biomedical Sciences, Federico II University of Naples, Italy.
§ Present address. Department of Cardiovascular Surgery, First Affiliated Hospital, College of Medicine, Zhejiang University, Zhejiang, China.

Graphical Abstract

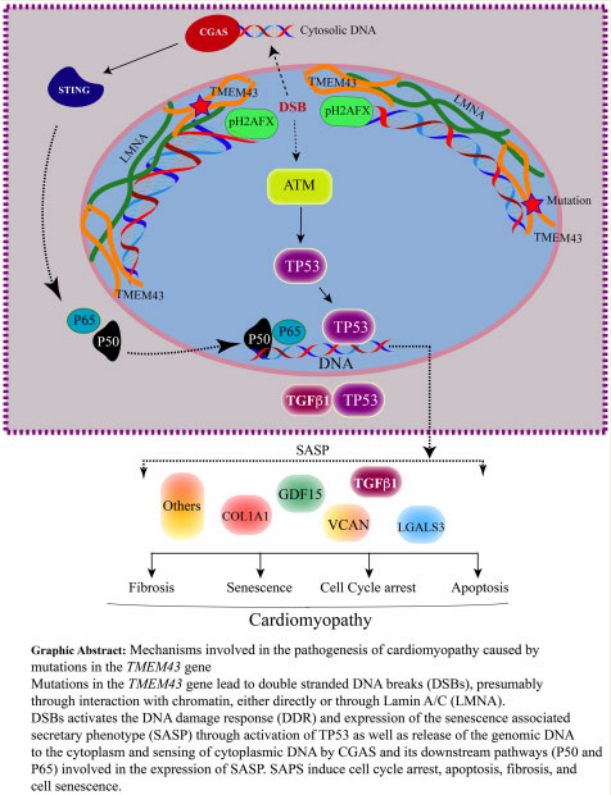

Graphic Abstract: Mechanisms involved in the pathogenesis of cardiomyopathy caused by mutations in the *TMEM43* gene
Mutations in the *TMEM43* gene lead to double stranded DNA breaks (DSBs), presumably through interaction with chromatin, either directly or through Lamin A/C (LMNA).
DSBs activates the DNA damage response (DDR) and expression of the senescence associated secretary phenotype (SASP) through activation of TP53 as well as release of the genomic DNA to the cytoplasm and sensing of cytoplasmic DNA by CGAS and its downstream pathways (P50 and P65) involved in the expression of SASP. SAPS induce cell cycle arrest, apoptosis, fibrosis, and cell senescence.

Keywords Cardiomyopathy • DNA damage • Senescence • Nuclear member proteins • Envelopathies

1. Introduction

Arrhythmogenic cardiomyopathy (ACM) encompasses a broad category of primary myocardial diseases whose manifestations are sudden cardiac death, ventricular arrhythmias, and heart failure.[1,2] Cardiac arrhythmias typically occur early and precede the onset of cardiac dysfunction or are judged to be disproportional to cardiac dysfunction, i.e. ventricular tachycardia occurs in the presence of mild cardiac dysfunction (reviewed in ref.[3]). This is in contrast to primary dilated cardiomyopathy (DCM), whose primary presentation is typically heart failure with cardiac arrhythmias typically occurring late in the course of the disease and commonly in the context of severe cardiac dysfunction. The classic form of ACM predominantly involves the right ventricle, particularly in the early stages, and is referred to as arrhythmogenic right ventricular cardiomyopathy (ARVC).[4] The pathological hallmark of the classic ARVC is progressive myocardial fibro-adipogenesis, with a predilection towards involvement of the right ventricle, which results in a gradual replacement of cardiac myocytes with fibro-adipocytes.[5]

ACM is a genetically heterogeneous disease. It was mainly recognized as the disease of desmosomes because of identification of mutations in several genes encoding desmosome proteins, namely *PKP2, DSP, DSG2, DSC2*, and *JUP*, encoding plakophilin 2, desmoplakin, desmoglein 2, desmocolin 2, and junction protein plakoglobin, respectively (reviewed in ref.[2]). Desmosomes are members of the intercalated disks (IDs), which are distinct structures at the cell–cell junctions in the myocardium. IDs are responsible for maintaining tissue mechanical integrity and are signalling hubs for pathways involved in mechano-sensing, including the canonical WNT and the Hippo pathways, which are implicated in the pathogenesis of ACM.[6–9]

The genetic spectrum of ACM has been recently expanded to include genes coding for proteins with a diverse array of functions. Notable among the recent findings are *CDH2*, which codes for cell adhesion protein cadherin 2; *CTNNA3* encoding ID protein αT-catenin; *FLNC*, which codes actin-binding protein filamin C; *PLN*, which codes for the calcium regulatory protein phospholamban; and *RBM20*, whose encoded protein targets sarcomere and calcium handling genes for splicing.[10–14] A propensity to cardiac arrhythmia, by definition, is a common feature of ACM caused by all causal genes, however, expression of other cardiac phenotypes, such as involvement of the chambers and myocardial histopathology seem to differ among patients with ACM. Whereas ARVC, the classic form of ACM, exhibits a predilection towards involvement of the right ventricle, ACM caused by mutations in the *FLNC* and *PLN* genes predominantly involve the left ventricle, not dissimilar from the classic DCM except for the preponderance of ventricular arrhythmias.[12,13]

Overall, phenotypic variability in ACM is in keeping with the variable expression of the phenotype in hereditary cardiomyopathies.

A distinct group of causal genes for ACM, specifically *LMNA* and *TMEM43*, encode nuclear inner membrane proteins lamin A/C (LMNA) and transmembrane protein 43 (TMEM43), respectively.[15,16] The human molecular genetic data provide robust evidence for the causal role of *LMNA* and *TMEM43* in ACM.[15–17] However, there are scant data on the molecular mechanisms by which mutations in the *TMEM43* gene cause ACM. It will not be surprising if distinct mechanisms are involved in the pathogenesis of ACM caused by mutations in genes encoding nuclear envelope proteins, such as TMEM43, as opposed to the subset caused by mutations in genes encoding desmosome proteins. Thus, the purpose of this study was to gain insights into the molecular mechanisms responsible for ACM caused by the *Tmem43* haploinsufficiency in mice.

2. Methods

An expanded Methods section is provided as Supplementary material online.

2.1 Data sharing and availability

RNA-seq data have been deposited in the public database GEO (https://www.ncbi.nlm.nih.gov/gds, GSE147317. Additional data pertaining to the present article are available from the corresponding author upon request.

2.2 Regulatory approvals

Animal procedures were in full compliance with the NIH Guidelines for the Care and Use of Laboratory Animals and approved by Animal Care and Use Committee of the University of Texas Health Science Center—Houston.

2.3 Anaesthesia and euthanasia

To isolate cardiac myocytes, mice were anaesthetized with intraperitoneal injection of a single dose (50 mg/kg) of pentobarbital. To perform echocardiography and electrocardiography, anaesthesia was induced with 3% inhaled isoflurane and was maintained at 0.5–1% isoflurane throughout the procedures. Mice were euthanized with CO_2 gas inhalation followed by cervical dislocation.

2.4 *Myh6-Cre:Tmem43*$^{W/F}$ mice

The *Tmem43* gene was deleted specifically in cardiac myocytes by crossing the *Myh6-Cre* deleter and *Tmem43*$^{tm1a(EUCOMM)Wtsi}$ mice (knock out mouse project—KOMP). The mouse contains a LacZ reporter cassette cloned into intron 4 of the *Tmem43* gene flanked by FLIPPASE recognition target (Frt) sites as well as floxed exons 5 to 7 of the *Tmem43* gene (Supplementary material online, *Figure S1*). One copy of the *Tmem43* gene was deleted in stepwise fashion, first upon excision of the LacZ reporter cassette using the mice expressing FLIPPASE and then excision of the floxed exon 5–7 of the *Tmem43* gene using the *Myh6-Cre* mice, as illustrated in Supplementary material online, *Figure S1*. Wild type and *Myh6-Cre* were also generated in the same genetic background and used as controls. Given that the genetic variants in the *TMEM43* gene, including truncation variants, in human patients with ACM are heterozygous mutations (https://www.ncbi.nlm.nih.gov/clinvar), only mice heterozygous for *Tmem43* deletion were generated and characterized. Mice were genotyped by PCR. Supplementary material online, *Table S1* lists sequence of the oligonucleotide primers used for genotyping and determining the recombination efficiency.

2.5 Cardiac size and function

Cardiac size and function were assessed using an ultrasound imaging system (Vevo 1100), equipped with a 22–55 MHz MicroScan transducer in age- and sex-matched littermates, as published.[18–21]

2.6 Gross morphology

Heart weight was measured after separation of the great vessels from the cardiac chambers and the heart weight was indexed to body weight.[18–21]

2.7 Myocardial fibrosis

Thin (5 micron) myocardial sections were cut from paraffin-embedded heart tissues and stained with picrosirius red or Masson's trichrome. Collagen volume fraction (CVF) was calculated as the percentage of picrosirius red stained area to total myocardial section area using ImageJ software, as published.[18–21]

2.8 Myocyte cross-sectional area

Thin myocardial sections were stained with Wheat Germ Agglutinin (WGA), as described previously.[19,22,23] To identify cardiac myocytes, myocardial sections were stained with an antibody against pericentriolar membrane protein (PCM1), which specifically marks the cardiac myocytes nuclei in the heart.[24,25] The number of cardiac myocytes and the areas stained for WGA were calculated in 6–12 microscopic fields per section and 6–10 sections per heart, comprising approximately 6000 to 12 000 myocytes per each mouse heart.[19]

2.9 Immunoblotting (IB)

Cardiac myocyte and whole heart protein extracts were analysed for expression of selected proteins by IB using ~50 μg aliquots of protein extracts, as published.[18–21] The list of primary antibodies and the respective horseradish linked secondary antibodies is provided in Supplementary material online, *Table S1*.

2.10 Immunofluorescence (IF)

Thin myocardial frozen sections were probed with specific primary antibodies and the corresponding conjugated secondary antibodies to detect expression and localization of the proteins of interest.[18–21] The list of the antibodies used for the IF studies is provided in Supplementary material online, *Table S1*.

2.11 TUNEL assay

Myocardial apoptosis was detected by terminal deoxynucleotidyl transferase dUTP nick end labelling (TUNEL) assay using the In-Situ Cell Death Detection Fluorescein Kit, as published.[18–20] Approximately, 6000 to 12 000 cells per each heart was analysed and the percentage of the TUNEL positive cells was calculated.

2.12 Isolation of adult mouse cardiac myocytes

Adult mouse cardiac myocytes were isolated using a collagenase perfusion method, as published.[19,20,26] In brief, the heart was perfused retrogradely with a digestion buffer containing collagenase type II (2.4 mg/mL) until it became spongy. The heart was then minced thoroughly to dissociate cells and the cell suspension was filtered through a

100 μm cell strainer. Cardiac myocytes were pelleted by centrifugation and subjected to step-wise exposure to increasing concentrations of calcium. Following the final wash, myocytes were used for RNA or protein isolation and immunostaining.

2.13 RNA sequencing (RNA-seq)

RNA-seq was performed as published.[18–20] In brief, total RNA was extracted from isolated ventricular cardiac myocytes and samples with an RNA Integrity Number (RIN) of >8 were used to prepare sequencing libraries. Samples were depleted from ribosomal RNA and strand-specific sequencing libraries were generated and sequenced on an Illumina HiSeq 4000 instrument to generate 75 bp paired-end reads. The sequencing reads were aligned to the mouse reference genome build mm10 using HISAT2.[27] The aligned read pairs were annotated using GENCODE gene model (https://www.gencodegenes.org/mouse/). Read counts were obtained using the featureCounts and the differential expression analysis was performed using the DESeq2 in the R package (https://www.r-project.org/).[28,29] Significance level was set at a *q*-value (Benjamini–Hochberg FDR-adjusted *P*-value) of <0.05.[30]

2.14 Pathway analysis

To identify the dysregulated biological pathways, the RNA-seq data were analysed for enriched gene sets using Ensemble of Gene Set Enrichment Analyses (EGSEA), which utilizes up to 12 prominent gene set testing algorithms and provides a combined ranking of enriched pathways and gene sets.[31] Significant pathways and gene sets were obtained based on combined $q < 0.05$ and presented based on combined ranks and scores.

Individual gene set analysis was performed using GSEA and significance was assessed by analysing signal-to-noise ratio and 1000 permutations against the curated gene sets for hallmark and the canonical pathways of Molecular signature database (MSigDB). The data were presented as enrichment score and an FDR cut-off of 0.05.

Differentially expressed genes (DEGs) were evaluated using the Ingenuity pathway analysis (IPA) software to predict their upstream regulators, which were categorized as the transcriptiona1 regulator (TRs) or growth factor. Activation or suppression of the upstream regulators was defined by determining the number of DEGs that overlapped with the curated genes in the specific pathway. A *P*-value of <0.05 and a Z score of greater than +2 or less than -2 were considered significant.

2.15 RT-PCR

Transcript levels of selected genes were quantified by RT-PCR. *Gapdh* transcript level was used to normalize the target gene expression level and the ΔΔCT method was used to compare the expression levels. The list of TaqMan probes and oligonucleotide primers used in the RT-PCR reactions are provided in Supplementary material online, *Table S1*.

2.16 Quantification of active TGFβ1 level

Active TGFβ1 protein levels were measured in cardiac myocytes using an ELISA kit. The assay was performed using 200 μg of the protein lysate upon activating the latent TGFβ1. TGFβ1 standards and samples were loaded on to pre-coated wells embedded with a TGFβ1-specific monoclonal antibody followed by incubation with an enzyme-linked polyclonal antibody specific for TGFβ1. TGFβ1 levels were quantified by the colorimetric detection method following addition of a substrate solution containing hydrogen peroxide and tetramethylbenzidine. Colour intensity of the reaction was determined using a Microplate reader. TGFβ1 level was calculated and plotted as pg/mg protein.

2.17 Co-immunoprecipitation (Co-IP)

Co-IP was performed as published with minor modifications.[32] In brief, adult mouse whole hearts were homogenized using a handheld homogenizer and the homogenates were incubated in a lysis buffer containing protease and phosphatase inhibitors. The lysates were disrupted by sonication using Bioruptor Pico and the supernatant was separated by centrifugation. Approximately 500 μg aliquot of each supernatant, after preclearing with protein G sepharose, was incubated with either an anti-TMEM43 or an anti-TGFβ1 antibody. The protein immune complexes were pulled down by protein G Sepharose beads, resolved on an SDS-PAGE gel, transferred to a membrane and probed with either an anti TMEM43 or an anti TGFβ1 antibody. The signal was detected using HRP conjugated secondary antibodies and the ECL western blotting detection kit in a LiCOR imager.

2.18 Cross-linked immunoprecipitation

The Co-IP studies were complemented with cross-linked immunoprecipitation, as described.[33] Briefly, aliquots of total heart tissues were cross-linked in 1% formaldehyde and sonicated to achieve fragment sizes of 200–500 bp. The fragments were precleared with Protein G Sepharose and incubated with 5 μg of an anti TMEM43 antibody or a control rabbit IgG. The immune complexes were pulled down with pre-coated BSA protein G Sepharose beads and resolved onto an SDS-polyacrylamide gel. Following transfer to a nitrocellulose membrane, the membrane was incubated with an anti LMNA or an anti TMEM43 antibody followed by incubation with an HRP conjugated secondary antibody. Signals were detected using the ECL western blotting detection kit with a LiCOR imaging system.

2.19 Protein phosphatase 2 (PP2A) activity assay

PP2A activity was measured in cardiac myocytes lysates using an Immunoprecipitation Phosphatase Assay Kit. To measure PP2A activity, PP2A was immunoprecipitated and assessed for phosphate release after addition of a phosphopeptide as a substrate. The reaction was detected with Malachite Green phosphate detection solution according to the manufacturer protocol. The absorbance values representing PP2A activity levels were measured using a microplate reader.

2.20 Statistical analysis

Gaussian distribution of the data was analysed by Shapiro–Wilk normality test. Data that followed a Gaussian distribution were compared by *t*-test or one-way analysis of variance (ANOVA) followed by Bonferroni pairwise comparisons. Data deviating from a Gaussian distribution were analysed by Kruskal–Wallis test. The categorical data were analysed by Fisher's exact or χ^2 test. Survival was analysed by Kaplan–Meier survival plots and the log-rank test. Statistical analyses were performed using Graph pad Prism 8 or STAT IC, 15.1.

3. Results

3.1 Expression and localization of TMEM43 protein in the mouse cardiac myocytes

To detect expression and subcellular localization of TMEM43 in cardiac myocytes, thin myocardial sections from WT mice were co-stained with antibodies against TMEM43 and PCM1, the latter is known to mark myocyte nuclei in the mouse heart.[24,25,34] Expression of TMEM43 was detected in 60.9 ± 7.4% of mouse cardiac myocytes in the myocardial sections (*Figure 1A*). Likewise, co-staining of isolated mouse cardiac myocytes with antibodies against TMEM43 and PCM1 detected expression and localization of TMEM43 protein to the nuclear membrane in the isolated cells (*Figure 1B*). Moreover, isolated myocytes were co-stained with antibodies against TMEM43 and LMNA, the latter is a nuclear inner membrane protein. TMEM43 and LMNA were co-stained and co-localized to myocyte nuclei, as shown in *Figure 1C*. Collectively, the data indicate expression and co-localization of TMEM43 protein to nuclear membrane in mouse cardiac myocytes, which is consistent with the data in the Human Protein Atlas (https://www.proteinatlas.org/ENSG00000170876-TMEM43).

To detect expression of TMEM43 in other myocardial cell types, thin myocardial sections were co-stained with antibodies against TMEM43 and LMNA or markers of fibroblasts (platelet-derived growth factor α—PDGFRA), smooth muscle cells (α smooth muscle actin—ACTA2), or endothelial cells (platelet and endothelial cell adhesion molecule 1—PECAM1). Co-staining of thin myocardial sections showed expression and nuclear co-localization of TMEM43 and LMNA proteins in the myocardium, as well as expression of TMEM43 protein in cardiac fibroblasts, smooth muscle cells, and endothelial cells (Supplementary material online, *Figure S2A–D*). Similarly, protein extracts from cardiac fibroblasts, endothelial cells, cells expressing platelet-derived growth factor receptor-α (PDGFRA), and pericytes were also probed with an anti TMEM43 antibody by immunoblotting. As shown in Supplementary material online, *Figure S2E*, TMEM43 was also expressed in other cardiac cell types.

3.2 *Myh6-Cre:Tmem43*$^{W/F}$ mice

The *Myh6-Cre:Tmem43*$^{W/F}$ mice were born per Mendelian expectations without notable abnormalities. Cre-mediated recombination efficiency in the DNA isolated from cardiac myocytes was determined by PCR using oligonucleotide primers upon amplification of the *Tmem43* floxed region (Supplementary material online, *Figure S3A*). Recombination efficiency, calculated as the fraction of *Tmem43* alleles that were recombined, was approximately 38.1 ± 4.6% in the *Myh6-Cre:Tmem43*$^{W/F}$ mouse myocytes (Supplementary material online, *Figure S3B*).

To determine efficiency of the deletion, *Tmem43* transcript and TMEM43 protein levels were determined by RT-PCR and immunoblotting, respectively, in cardiac myocytes isolated from the WT, *Myh6-Cre*, and *Myh6-Cre:Tmem43*$^{W/F}$ mice. *Tmem43* transcript levels were reduced by ∼40% in the *Myh6-Cre:Tmem43*$^{W/F}$ myocytes as compared to the WT myocytes and were unchanged in the *Myh6-Cre* mice alone (*Figure 1D*). Likewise, TMEM43 protein levels were reduced by 30.6 ± 9.5 in cardiac myocytes isolated from the *Myh6-Cre:Tmem43*$^{W/F}$ mice (*Figure 1E and F*). There were no differences in the TMEM43 protein levels in cardiac myocytes isolated from the WT and *Myh6-Cre* mice (Supplementary material online, *Figure S4*). TMEM43 protein levels in the whole heart were not significantly different between the *Myh6-Cre:Tmem43*$^{W/F}$ and WT mice, consistent with expression of the TMEM43 protein in other cardiac cell types, masking reduced TMEM43 level in the myocytes (*Figure 1G and H*).

3.3 Gross cardiac morphology and survival

Myh6-Cre:Tmem43$^{W/F}$ appeared grossly normal but died prematurely between 4 and 17 months, resulting in a median survival of ∼12 months (*Figure 1I*). The WT and *Myh6-Cre* mice had survival rates of 95% and 90%, respectively at ∼20 months (*Figure 1I*). The ventricular weight/body weight ratio was increased in the *Myh6-Cre:Tmem43*$^{W/F}$ mice as compared to WT or *Myh6-Cre* mice (*Figure 1J*). Considering survival rate of the *Myh6-Cre:Tmem43*$^{W/F}$ mice, subsequent phenotypic characterization was performed at ∼4 and ∼9 months of life.

3.4 Serial evaluation of cardiac dimensions and function

The *Myh6-Cre:Tmem43*$^{W/F}$ mice did not exhibit a discernible echocardiographic phenotype at 4 months of age, as indices of cardiac size and function were normal (Supplementary material online, *Table S2*). However, the *Myh6-Cre:Tmem43*$^{W/F}$ mice developed left ventricular (LV) dilatation and dysfunction by 9 months of age (*Table 1*). Accordingly, LV end-diastolic diameter and end-systolic diameter were increased and LV fractional shortening was reduced by about 50%, as compared to sex- and age-matched WT and *Myh6-Cre* mice (*Table 1*). In conjunction with these changes, LV mass and LV mass indexed to body weight were increased. There was no discernible echocardiographic phenotype in the *Myh6-Cre* mice (*Table 1*).

3.5 Myocardial fibro-adipogenesis

To detect myocardial fibrosis, thin myocardial sections were stained with picrosirius red or Masson's trichrome at two-time points of 4 and 9 months of age. CVF, determined as the percent of the myocardial sections stained for picrosirius red, was similar among the experimental groups at ∼4 months of age (Supplementary material online, *Figure S5A* and *B*). However, CVF was markedly increased in 9 months old *Myh6-Cre:Tmem43*$^{W/F}$ mouse hearts, comprising about 3 to 10% of the myocardium, whereas it was <2% in the age- and sex-matched WT and *Myh6-Cre* mouse hearts (*Figure 2A and B*). Masson's trichrome staining also showed patchy areas of myocardial fibrosis in the *Myh6-Cre:Tmem43*$^{W/F}$ mice (*Figure 2C*). In accord with these findings, transcript levels of several genes coding for the markers of fibrosis, namely *Col1a1, Col3a1, Tgfb1, Tgfb2, Ctgf*, and *Timp1* were increased in the hearts of *Myh6-Cre:Tmem43*$^{W/F}$ mice as compared to WT or *Myh6-Cre* mice (*Figure 2D*).

To assess adipogenesis in the heart, fresh frozen myocardial sections were immunostained for the expression of the adipogenic transcription factor CEBPA and the percentage of nuclei expressing CEBPA was determined in approximately 42 000 cells per genotype. The number of nuclei stained positive for the expression of CEBPA was increased significantly in the *Myh6-Cre:Tmem43*$^{W/F}$ mouse hearts as compared to WT or *Myh6-Cre* controls (*Figure 2E and F*). In addition, thin myocardial sections were stained with an antibody against perilipin 1 (PLIN1), a specific marker for lipid-rich adipocytes, which showed increased number of adipocytes in the *Myh6-Cre:Tmem43*$^{W/F}$ as compared to *Myh6-Cre* or WT mouse hearts (*Figure 2G and H*). Moreover, the number of cells containing oil droplets, as detected by Oil Red O (ORO) staining of thin myocardial section, was increased in the *Myh6-Cre:Tmem43*$^{W/F}$ hearts at 9 but not at 4 months of age as

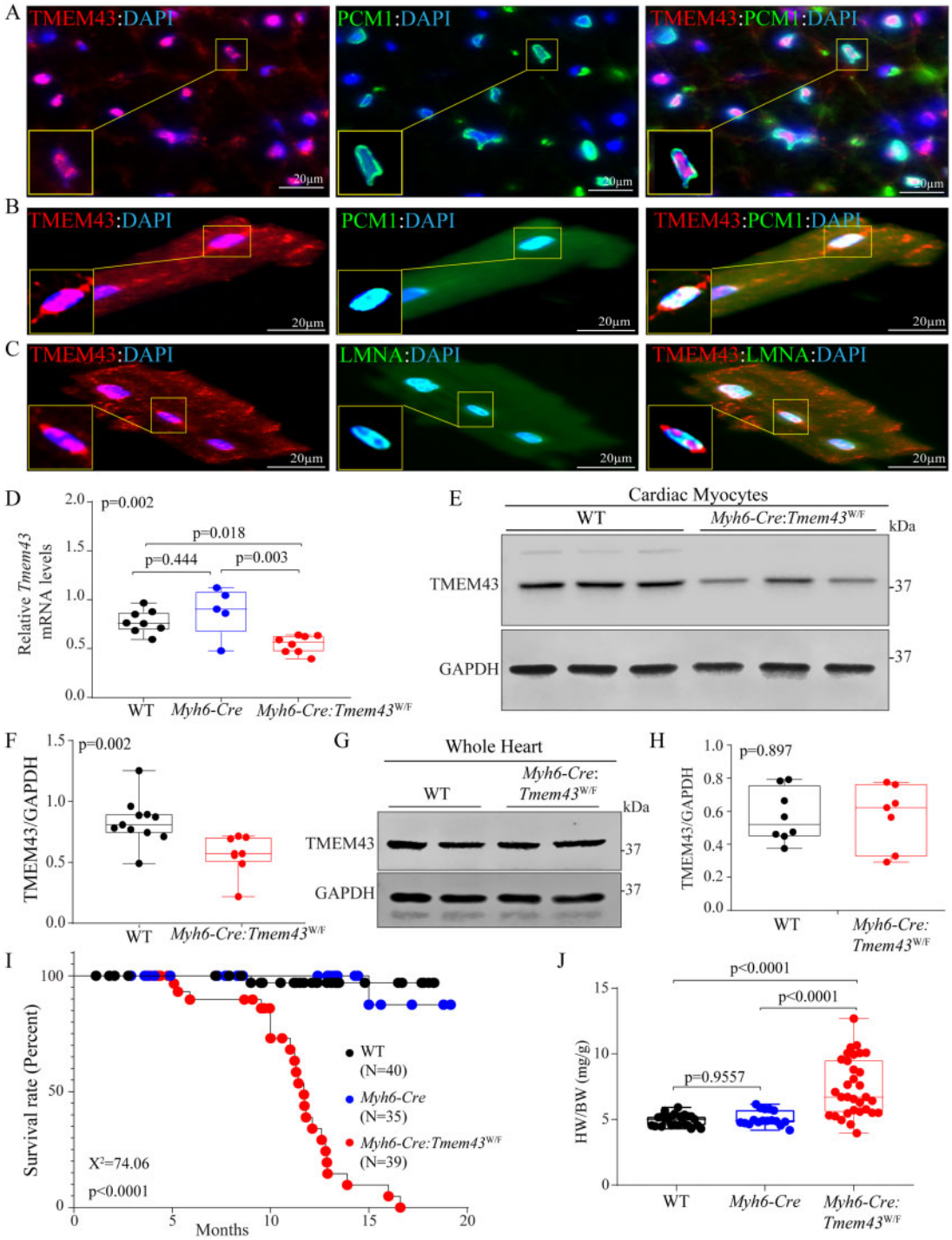

Figure 1 TMEM43 expression, localization, and deletion in mouse cardiac myocytes. (*A*) TMEM43 expression and localization to myocyte nuclear membrane illustrated in thin myocardial sections from wild-type mice upon co-staining of myocardial sections with antibodies against TMEM43 (red) and PCM1 (green), the latter being a specific marker of cardiac myocytes nuclei. The nuclei were counter stained with DAPI (blue). (*B* and *C*) Co-staining of isolated cardiac myocytes from wild-type mice for TMEM43 and PCM1 (*B*) or TMEM43 and LMNA (*C*). Nuclei are stained with DAPI. (*D*) Reverse transcription-quantitative PCR (RT-PCR) showing reduced *Tmem43* transcript levels by ∼40% in the *Myh6-Cre:Tmem43*$^{W/F}$ cardiac myocytes. ANOVA followed by pairwise *P*-values are depicted (N = 5–8 per group). (*E*) Immunoblotting (IB) showing reduced TMEM43 protein levels in the *Myh6-Cre:Tmem43*$^{W/F}$ as compared to the WT cardiac myocytes. (*F*) Quantitative data of TMEM43 protein levels, showing reduced levels in the *Myh6-Cre:Tmem43*$^{W/F}$ as compared to WT cardiac myocytes. N = 8–10 per group, *P*-value was obtained by *t*-test. (*G* and *H*) IB and the corresponding quantitative data (normalized to GAPDH) showing unchanged TMEM43 protein levels in whole heart protein extracts in the *Myh6-Cre:Tmem43*$^{W/F}$ as compared to WT mice (N = 7 per group, *P*-value was determined by unpaired *t*-test). (*I*) Kaplan–Meier survival plots showing reduced survival rate in the *Myh6-Cre:Tmem43*$^{W/F}$ as compared to the WT and *Myh6-Cre* mice (N = 35–40 per group, log-rank test *P*-value is shown). (*J*) Increased heart weight to body weight ratio in the *Myh6-Cre:Tmem43*$^{W/F}$ as compared to mice in the control groups (N = 20–31 per group, ANOVA and pairwise *P*-values are depicted).

Table 1 Echocardiographic findings in the *Myh6-Cre:Tmem43* $^{W/F}$ and control mice

	WT	*Myh6-Cre*	*Myh6-Cre: Tmem43* $^{W/F}$	*P*-value
N (male/female)	16 (6/10)	13 (4/9)	20 (12/8)	0.1972*
Age (m)	9.3 ± 1.20	8.4 ± 1.90	8.7 ± 2	0.33
BW (g)	30.4 ± 7.50	30.2 ± 7.60	28.3 ± 5.10	0.5932
HR (b.p.m.)	520.2 ± 43.40	497 ± 38.90	522 ± 50	0.2817
ST (mm)	0.7 ± 0.07	0.7 ± 0.10	0.7 ± 0.10	0.8248
LVEDD (mm)	3.5 ± 0.30	3.6 ± 0.40	4.1 ± 0.80**&	0.0039
LVEDDi (mm/g)	0.12 ± 0.02	0.13 ± 0.03	0.15 ± 0.04**&	0.0086
PW (mm)	0.78 ± 0.10	0.8 ± 0.10	0.8 ± 0.10	0.9818
LVESD (mm)	2.1 ± 0.40	2.4 ± 0.30	3.4 ± 1**&	<0.0001
FS (%)	39 ± 7.80	33.1 ± 3.90	19.1 ± 9.60**&	<0.0001
EF (%)	69.6 ± 9.60	62.4 ± 5.20	38.6 ± 17.50**&	<0.0001
LVM (mg)	71.3 ± 19.40	73.2 ± 14.60	94.2 ± 31.80**&	0.0019
LVMi (mg/g)	2.3 ± 0.60	2.5 ± 0.70	3.4 ± 1.20**&	0.0065

BW, body weight; FS, fractional shortening; HR, heart rate; IVST, interventricular septum thickness; LVEDD, left ventricular end-diastolic diameter; LVEDDi, LVEDD indexed to the body weight; LVESD, left ventricular end-systolic diameter; LVM, left ventricular mass; LVMI, LVM indexed to the body weight; LVPWT, left ventricular posterior wall thickness; M/F, male/female; Myh6-Cre and WT, controls; *Myh6-Cre:Tmem43* $^{W/F}$, cardiac myocyte specific heterozygous deletion of *Tmem43*.
*X^2 test.
P-values were obtained by one-way ANOVA followed by Bonferroni pairwise comparisons.
**$P < 0.05$ vs. WT.
&$P < 0.05$ vs. *Myh6-Cre*.

compared to the corresponding control groups (*Figure 2I and J* and Supplementary material online, *Figure S5C* and *D*).

To corroborate the histological findings, transcript levels of several genes involved in adipogenesis were quantified by RT-PCR. Transcript levels of *Cebpa, Apoe, Dgat1*, and *Ucp1* were significantly increased in the *Myh6-Cre:Tmem43* $^{W/F}$ hearts, whereas transcript levels of *Adipoq* and *Pparg* were unchanged as compared to levels in WT or *Myh6-Cre* hearts (*Figure 2K*).

3.6 Apoptosis

Apoptosis was assessed by TUNEL assay at two-time points of 4 and 9 months of age. Whereas the number of TUNEL positive cells in the heart was not increased at 4 months of age, the number of myocardial cells stained positive for the TUNEL assay was increased by about three-fold at 9 months of age in the *Myh6-Cre:Tmem43* $^{W/F}$ mice, as compared to the WT or *Myh6-Cre* mice (*Figure 3A and B* and Supplementary material online, *Figure S5E* and *F*). In accord with the increased number of TUNEL positive cells, transcript levels of several genes encoding selected markers of apoptosis, including *Bnip3, Gadd45b, Gadd45g, Cdkn1a*, and *Noxa* were increased whereas the increase in the transcript levels of *Bax* was of borderline significance, and those of *Bcl2l11* were decreased in the *Myh6-Cre:Tmem43* $^{W/F}$ hearts compared to the control groups (*Figure 3C*). In contrast, transcript levels of anti-apoptosis gene *Bcl2* and *Puma* were not different among the experimental groups (*Figure 3C*). To corroborate the findings, levels of the cleaved caspase 3 (CASP3) were analysed in myocardial protein extracts, which were increased in the *Myh6-Cre:Tmem43* $^{W/F}$ hearts as compared to control hearts (*Figure 3D and E*). Finally, to determine whether cardiac myocytes or fibroblasts are undergoing apoptosis, protein extracts from cardiac myocytes and fibroblasts were probed for the expression of cleaved and total CASP3. Cleaved CASP3 protein was detected in myocyte and whole heart protein extracts but not in the protein extracts from cardiac fibroblasts (*Figure 3F*). Only full-length CASP3 was detected in cardiac fibroblasts in the *Myh6-Cre:Tmem43* $^{W/F}$ mice (*Figure 3F*).

3.7 Cardiac myocyte size

To quantify myocyte cross-sectional area (CSA), thin myocardial sections were co-stained with WGA to mark the cell boundaries and PCM1 to tag myocyte nuclei. The number of cells expressing PCM1, i.e. cardiac myocytes, was reduced in the *Myh6-Cre:Tmem43* $^{W/F}$ hearts (*Figure 3G and H*). Myocyte CSA, as determined from the areas stained for WGA and corrected for the number of cardiac myocytes, was significantly increased in *Myh6-Cre:Tmem43* $^{W/F}$ mouse hearts as compared to WT and *Myh6-Cre* mouse hearts (*Figure 3I and J*). Likewise, transcript levels of selected markers of cardiac hypertrophy, including *Nppa, Nppb, Acta2*, and *Myh7* were increased (*Figure 3K*), while that of *Atp2a2* (Serca2a) was reduced in the *Myh6-Cre:Tmem43* $^{W/F}$ as compared to control mice in accord with histology findings (*Figure 3L*). *Myh6* transcript levels were unchanged (*Figure 3L*). Thus, the molecular phenotype is in accord with the expression of myocyte hypertrophy and cardiac systolic dysfunction in the *Myh6-Cre:Tmem43* $^{W/F}$ mice.

3.8 Serial cardiac myocyte RNA-seq

Cardiac myocyte transcripts from age- and sex-matched WT and *Myh6-Cre:Tmem43* $^{W/F}$ mice were analysed by RNA-seq at two time points of 4 and 9 months of age, defined as pre- and post-cardiac dysfunction, respectively. The time points were selected based on echocardiographic determination of cardiac function (Supplementary material online, *Tables S2* and *S3*). The early time point (4 months) enabled identification of transcriptomic changes that occur early and precede the onset of cardiac phenotype, including cardiac dysfunction, whereas the late time point (9 months) provided the opportunity to detect cardiac myocyte transcriptomic changes in mice with established phenotype.

A total of 483 genes were differentially expressed at 4 months of age, as depicted in the volcano plot and the corresponding heat map (*Figure 4A and B*). The corresponding number of the DEGs in cardiac myocytes isolated from the 9 months old *Myh6-Cre:Tmem43* $^{W/F}$ mice was 1005 genes, which were comprised of 558 up-regulated and 447 down-regulated genes, as compared to the WT myocytes (*Figure 4C and D*). The two sets of the DEGs were analysed to detect temporal changes in gene expression that coincide with evolution of cardiac phenotype in the *Myh6-Cre:Tmem43* $^{W/F}$ mice. A total of 133 genes were differentially expressed at both time points in the *Myh6-Cre:Tmem43* $^{W/F}$ myocytes as compared to the corresponding WT myocytes, whereas 350 and 872 DEGs were exclusive to 4 and 9 month-time points, respectively (*Figure 4E*). The heat map representing DEGs exclusive to the 9 months old *Myh6-Cre:Tmem43* $^{W/F}$ myocytes is shown in *Figure 4F*.

To validate the RNA-seq findings, transcript levels of 55 DEGs (42 and 13 genes at 4- and 9-month time points, respectively) in the RNA-seq data were quantified by RT-PCR in independent biological samples. The results of the RT-PCR experiment at each time point were concordant with the corresponding results of RNA-seq (*Figure 4G–L*). Accordingly, fold changes in the transcript levels of the selected genes in the *Myh6-Cre:Tmem43* $^{W/F}$ myocytes, determined by RNA-seq and RT-

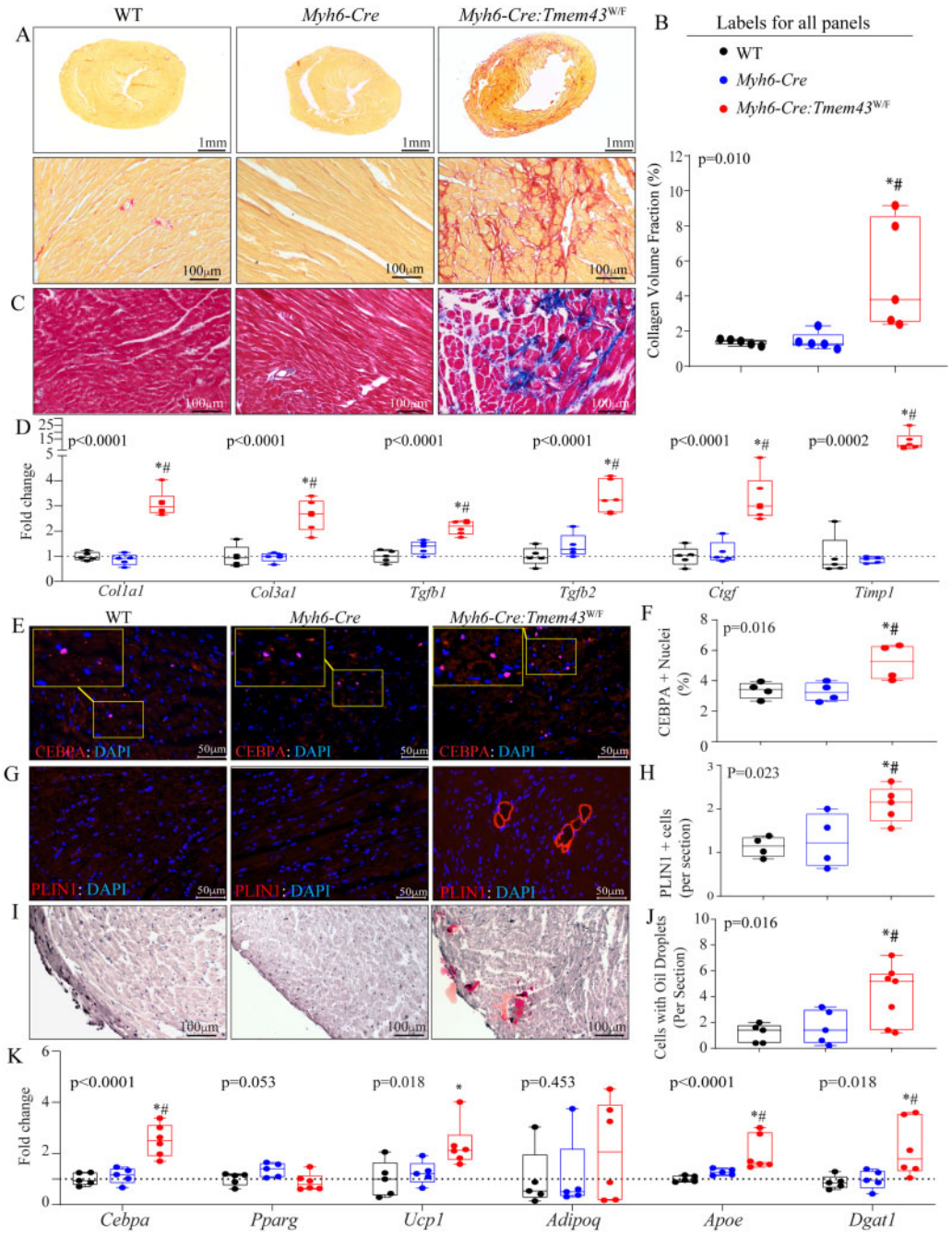

Figure 2 Myocardial fibrosis and adipogenesis *in 9 months old Myh6-Cre:Tmem43*$^{W/F}$ mice. (*A*) Representative low (upper) and high (lower) magnification panels of thin myocardial sections, stained with Picrosirius Red, showing increased fibrosis in the *Myh6-Cre:Tmem43*$^{W/F}$ mice. (*B*) Quantitative analysis of fibrosis, presented as Collagen Volume Fraction (CVF), exhibiting increased fibrosis in the *Myh6-Cre:Tmem43*$^{W/F}$ mice (n = 5 per group; ANOVA P = 0.010, *P = 0.020 vs. *Myh6-Cre*, $^{\#}P$ = 0.018 vs. WT). (*C*) Representative image of Masson's trichrome staining, corroborating increased fibrosis in the *Myh6-Cre:Tmem43*$^{W/F}$ mice. (*D*) Transcript levels of selected markers of fibrosis in the heart showed increased levels in the *Myh6-Cre:Tmem43*$^{W/F}$ mice (n = 5; ANOVA P-value is shown; * denotes P-value ≤0.05 between WT and *Myh6-Cre:Tmem43*$^{W/F}$, and # denotes P-value ≤0.05 between *Myh6-Cre* and *Myh6-Cre:Tmem43*$^{W/F}$ mice). (*E* and *F*) Immunofluorescence panels stained for CEBPA using an anti-CEBPA antibody (*E*) and the corresponding quantitative analysis (*F*) showing increased number of cells expressing CEBPA in the *Myh6-Cre:Tmem43*$^{W/F}$ myocardium as compared to WT and *Myh6-Cre* mice (n = 4 per group; ANOVA P = 0.016, *P = 0.023 vs. *Myh6-Cre*, $^{\#}P$ = 0.031 vs. WT). (*G* and *H*) Immunofluorescence panels showing myocardial sections stained for PLIN1, a specific marker of lipid containing adipocytes (*G*) and the corresponding quantitative data (*H*), showing increased number of adipocytes in the *Myh6-Cre:Tmem43*$^{W/F}$ myocardium (n = 4 or 5 per group; ANOVA P = 0.023, *P = 0.049 vs. *Myh6-Cre*, $^{\#}P$ = 0.023 vs. WT). (*I* and *J*) Oil Red O stained thin myocardial sections in 9 months old mice (*I*) and the corresponding quantitative data (*J*), shown as number of cells with oil droplets per section, indicated increased fat infiltration in the heart of the *Myh6-Cre:Tmem43*$^{W/F}$ mice (n = 5; ANOVA P = 0.016, *P = 0.056 vs. *Myh6-Cre*, $^{\#}P$ = 0.023 vs. WT). (*K*) Transcript levels of adipogenic genes, analysed by RT-PCR, showing increased levels of *Cebpa* (P < 0.0001), *Ucp1* (P = 0.018), *Apoe* (P = 0.0001), and *Dgat1* (P = 0.018) in the heart of 9 months old *Myh6-Cre:Tmem43*$^{W/F}$ mice (n = 5; P-value shown denotes ANOVA P-value between the three groups, * denotes P-value ≤0.05 between WT and *Myh6-Cre:Tmem43*$^{W/F}$, and # denotes P-value ≤0.05 between *Myh6-Cre* and *Myh6-Cre:Tmem43*$^{W/F}$ mice). Differences among the three groups were compared by one-way ANOVA.

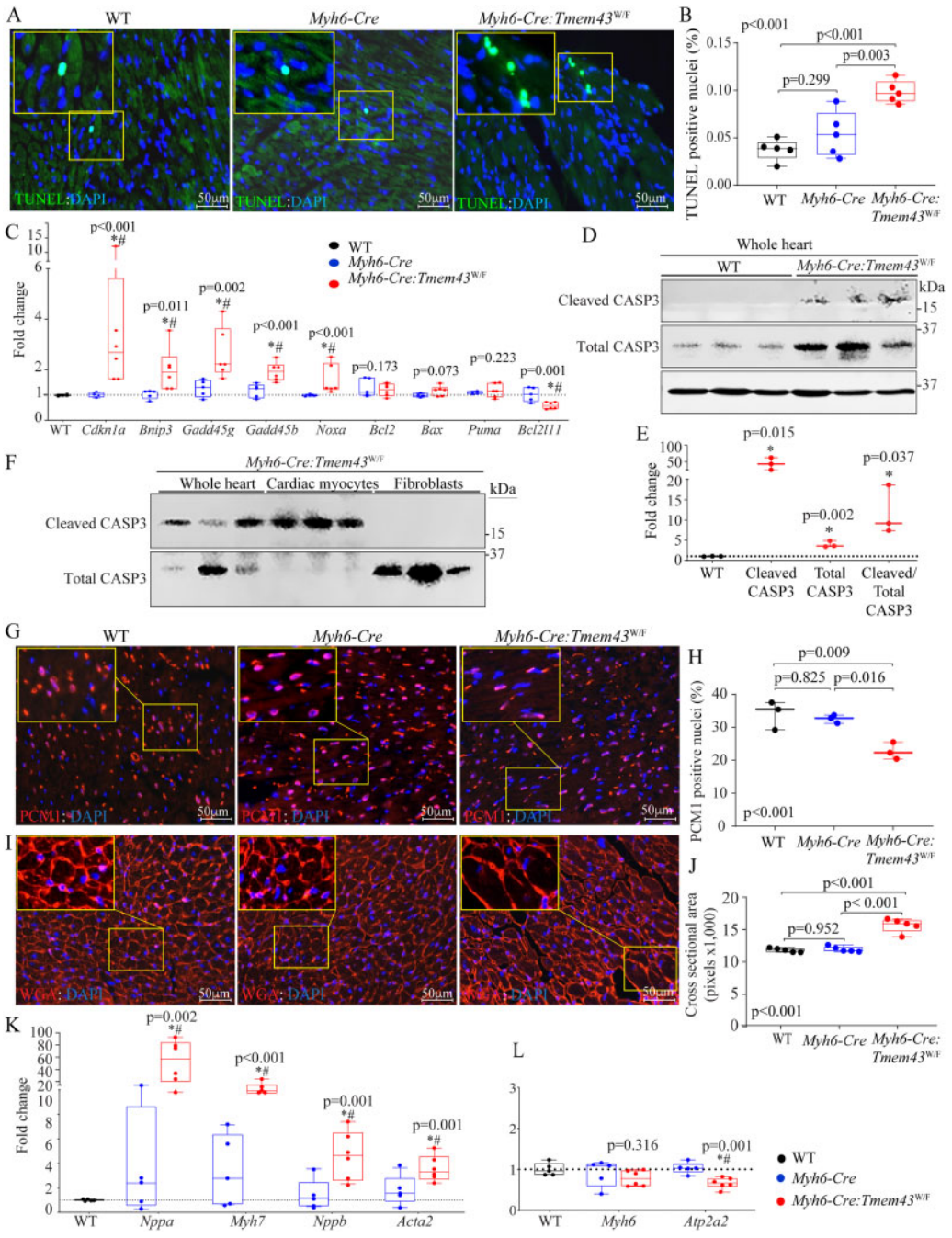

Figure 3 Myocardial apoptosis and cardiac hypertrophy in 9 months old *Myh6-Cre:Tmem43*$^{W/F}$ mice. (*A*) Representative images of Terminal deoxynucleotidyl transferase dUTP nick end labelling (TUNEL) assay showing apoptotic cells in the heart of the *Myh6-Cre:Tmem43*$^{W/F}$ mice. (*B*) Quantitative analysis of TUNEL assay showing increased number of apoptotic cells in the heart of *Myh6-Cre:Tmem43*$^{W/F}$ mice ($N = 5$ per group, ANOVA followed by pairwise *P*-values are depicted). (*C*) Transcript levels of selected markers of apoptosis in the heart, analysed by RT-PCR, showing increased levels of *Cdkn1a, Bnip3, Gadd45g, Gadd45b*, and *Noxa* and decreased levels of *Bcl2l11* in the *Myh6-Cre:Tmem43*$^{W/F}$ as compared to WT or *Myh6-Cre* myocytes. Levels of *Bcl2*, *Bax*, and *Puma* were unchanged ($N = 6$ per group, *P*-values by unpaired *t*-test). (*D* and *E*) Detection of cleaved caspase 3 (CASP3) in the heart. Immunoblots (*D*) and quantitative data showing increased levels of cleaved (active) CASP3 in the heart of *Myh6-Cre:Tmem43*$^{W/F}$ mice. ($N = 3$ per group, *P*-values were determined by *t*-test). (*F*) Detection of cleaved CASP3 in the whole heart, isolated myocytes and isolated fibroblasts from the *Myh6-Cre:Tmem43*$^{W/F}$ mouse hearts. Cleaved CASP3 is detected in the whole heart and isolated myocytes but not fibroblasts. (*G* and *H*) Immunofluorescence panels showing staining for PCM1, a cardiac myocyte specific nuclear marker used to calculate the number of cardiac myocytes. Quantitative data of PCM1 staining showing decreased number of cardiac myocytes in the *Myh6-Cre:Tmem43*$^{W/F}$ mouse hearts ($N = 3$ per group, ANOVA and pairwise comparisons). (*I* and *J*) Panels representing thin myocardial sections stained for Wheat Germ Agglutinin (WGA) showing increased cardiac myocytes cross-sectional area in the *Myh6-Cre:Tmem43*$^{W/F}$ mouse heart (*I*) and the corresponding quantitative data (*J*, $N = 5$ per group, ANOVA followed by pairwise comparisons). (*K* and *L*) RT-PCR analysis of selected markers of cardiac hypertrophy and myocardial dysfunction showing increased transcript levels of *Nppa, Nppb, Acta2*, and *Myh7* (*K*) and decreased *Myh6* and *Atp2a2* transcript levels (*L*) in the heart of *Myh6-Cre:Tmem43*$^{W/F}$ mice, as compared to controls ($N = 6$ per group, ANOVA and *t*-test *P*-values are presented).

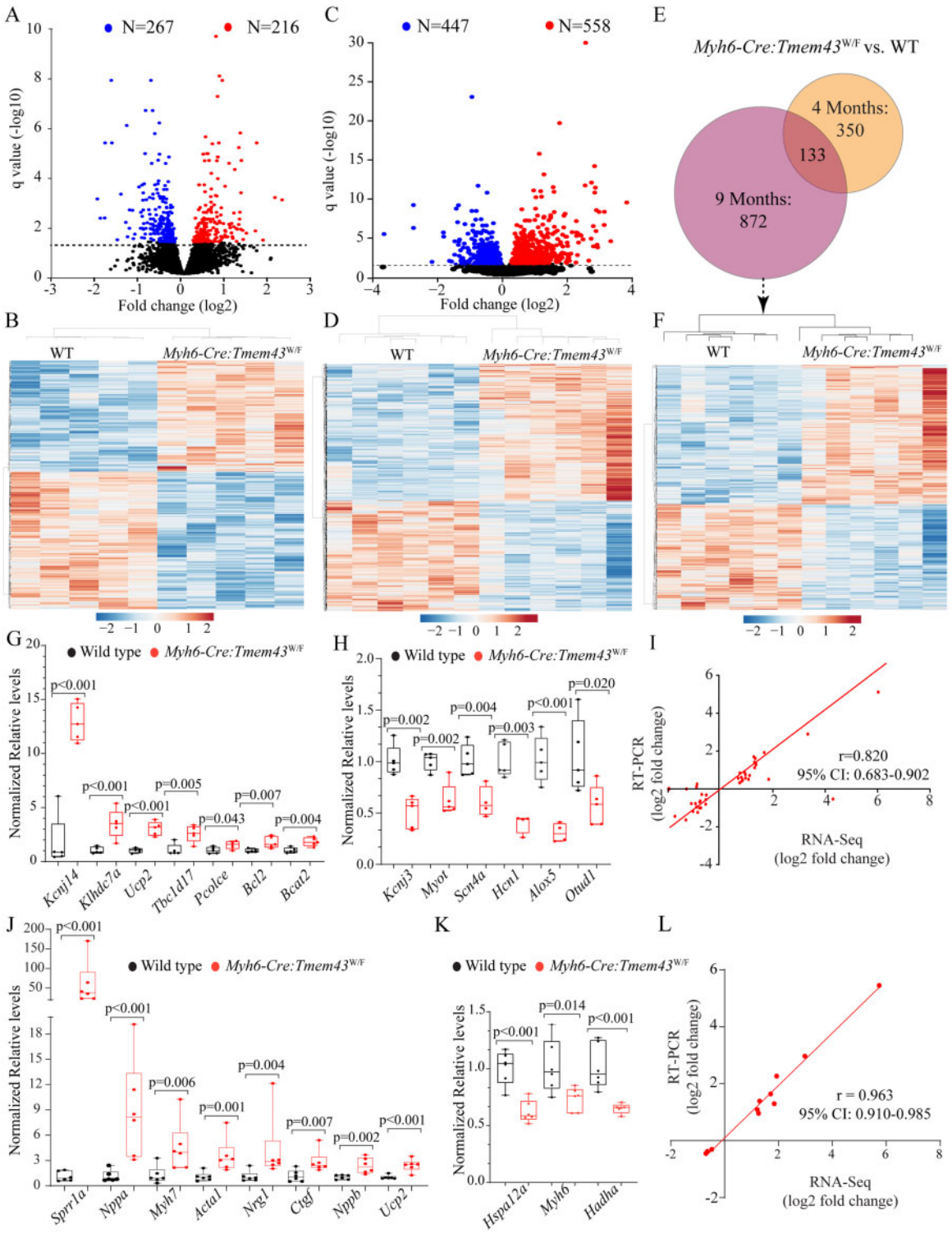

Figure 4 Cardiac myocytes transcriptome in the *Myh6-Cre:Tmem43*$^{W/F}$ mice. (*A* and *B*) Volcano plot and heat map showing differentially expressed genes (DEGs) in cardiac myocytes isolated from 4 months old WT and *Myh6-Cre:Tmem43*$^{W/F}$ mice ($N = 5$ per group). The dash line indicates significance level at $q < 0.05$. Blue indicate down-regulated, red up-regulated, and black unchanged transcripts. (*C* and *D*) Volcano plot and heat map showing DEGs in cardiac myocytes isolated from 9 months old WT and *Myh6-Cre:Tmem43*$^{W/F}$ mice ($N = 6$ per group). (*E*) Venn diagram showing comparison of the DEGs at 4 and 9 months of age, which identifies DEGs common to both time points or exclusive to one. (*F*) The heat map illustrates DEGs that were exclusive to the 9 months old *Myh6-Cre:Tmem43*$^{W/F}$ myocytes. (*G–I*) RT-PCR data showing transcript levels of top 14 DEGs, including 7 up-regulated (G) and 6 down-regulated (H), in independent samples collected at 4 months of age ($N = 5$ per group, unpaired *t*-test *P*-values). Fold changes in gene expression showed strong correlation between RNA-Seq and RT-PCR in two sets of independent biological samples for 42 DEGs (*I*, Spearman $\rho = 0.820$). (*J–L*) Validation of the top DEGs, up-regulated (*J*) and down-regulated (*K*) at 9 months old myocytes in independent biological samples by RT-PCR showing concordant results ($N = 6$ per group, unpaired *t*-test *P*-values) and the correlation between the two sets of data showing a strong correlation (*L*, Spearman $\rho = 0.868$).

PCR experiments were strongly correlated at each time point (Spearman $r = 0.820$ and $r = 0.963$ at 4 and 9 months, respectively, *Figure 4I and L*). A complete list of DEGs ($q < 0.05$) has been submitted to Gene Expression Omnibus (GSE147317).

The DEGs in the *Myh6-Cre:Tmem43*$^{W/F}$ myocytes at each time point were analysed by IPA to detect enrichment for the targets of the TRs. At the pre-cardiac dysfunction time point (4 months), only targets of the TP53 were enriched (Z score: 2.3), predicting activation of this major pathway (Supplementary material online, *Figure S6A*). Enrichment of the TP53 target genes was further pronounced upon evolving of cardiac phenotype in the 9 months old mice (Supplementary material online, *Figure S6A*). There was a modest decrease in the MAFB transcriptional output, suggesting its suppression (Supplementary material online, *Figure S6B*). In contrast, at 9 month-timepoint, targets of several TRs, in addition to TP53, were enriched, including ATF4, MRTFA, and MEF2D (Supplementary material online, *Figure S6C*). Likewise, DEGs predicted suppression of transcriptional activities of PPARGC1A, SMAD7, KLF15, and others (Supplementary material online, *Figure S6D*). A similar analysis for the growth and mitotic factors showed marked activation of several factors at 9 months of age, particularly TGFB1, ANGP2, and AGT, as depicted in Supplementary material online, *Figure S6E–G*.

GSEA analysis of the DEGs at 4 months of age showed enrichment of genes pertaining to biological pathways involved in protein synthesis and oxidative phosphorylation (Supplementary material online, *Figure S7*). A similar analysis of the DEGs at 9 months of age-predicted activation of epithelial–mesenchymal transition (EMT), inflammation, and apoptosis, and suppression of oxidative phosphorylation, adipogenesis and the metabolic signalling pathways (Supplementary material online, *Figure S7*).

3.9 Validation of the TP53 pathway activation

Given the prominence of the TP53 pathway among the dysregulated TRs, the pathway was further analysed. At 4 months of age, there were modest increases in levels of total TP53, phospho(S18)-TP53 and phospho(389)-TP53 proteins in cardiac myocyte protein extracts from the *Myh6-Cre:Tmem43*$^{W/F}$ mice as compared to the WT (Supplementary material online, *Figure S8*). Levels of selected proteins in the DNA damage response (DDR), namely; CGAS, STING1, total H2AFX, and pH2AFX, were not significantly changed (Supplementary material online, *Figure S8*). However, at 9 months of age, multiple lines of evidence indicated activation of the TP53 pathway. The heat map of the TP53 target genes illustrated changes consistent with activation of the TP53 in the *Myh6-Cre:Tmem43*$^{W/F}$ myocytes (*Figure 5A*). The dysregulated biological pathways pertaining to the TP53 pathway are depicted in *Figure 5B*. Transcript levels of genes involved in cell death, extracellular matrix, cell cycle, and oxidative stress were dysregulated (*Figure 5B*). The findings of the RNA-seq experiments showing dysregulated TP53 targets were tested for validation by analysing transcript levels of 20 selected genes by RT-PCR in independent biological samples. The changes were concordant with those in the RNA-seq data, as all showed changes in the same direction by both methods (*Figure 5C and D*). Consequently, there was a strong correlation between changes in the transcript levels of the selected genes in the *Myh6-Cre:Tmem43*$^{W/F}$ myocytes by the two methods (Pearson $r^2 = 0.89$, *Figure 5E*). Furthermore, immunoblotting was performed on cardiac myocyte protein extracts using an anti-TP53 antibody, which detected increased TP53 total protein levels (*Figure 5F and G*). Similarly, levels of phosphorylated TP53 (S18 and S389, corresponding to S15 and S392 in the human TP53, respectively) were increased in cardiac myocytes protein extracts from the *Myh6-Cre:Tmem43*$^{W/F}$ mice (*Figure 5F and G*). Likewise, levels of CDKN1A (p21) protein, a bona-fide TP53 target, were increased in the *Myh6-Cre:Tmem43*$^{W/F}$ myocyte protein extracts (*Figure 5H and I*). Collectively, the data provide multiple evidence of activation of the TP53 pathway.

3.10 Increased DDR and SASP

TP53, considered a guardian of the genome, is known to be activated in response to DNA damage (reviewed in ref.35). In addition, TP53 is activated in cardiomyopathies caused by mutation in the *LMNA* gene, encoding a nuclear envelope protein.[18] In view of the data establishing TMEM43 as a nuclear envelope protein, activation of the DDR pathway was analysed in the *Myh6-Cre:Tmem43*$^{W/F}$ myocytes. Immunoblotting showed increased levels of phospho- (S1981) and total ATM (Ataxia Telangiectasia mutated), an archetypical DDR protein and a major regulator of TP53, in the *Myh6-Cre:Tmem43*$^{W/F}$ myocyte extracts (*Figure 6A and B*).[36] Likewise, levels of CGAS protein, as sensor of cytoplasmic DNA, and its downstream molecule STING1 (TMEM173) were increased (*Figure 6A and B*). Moreover, levels of phospho-histone H2AFX, which is activated in response to double stranded DNA breaks (DSBs) were increased as detected by immunoblotting of myocardial protein extracts as well as IF staining of thin myocardial sections (*Figure 6A and B*). Furthermore, immunofluorescence staining of thin myocardial sections detected an increased number of nuclei expressing pH2AFX in the *Myh6-Cre:Tmem43*$^{W/F}$ hearts (*Figure 6C and D*).

A hallmark of activation of the DDR/TP53 pathway is context-dependent increased expression of a set of secreted proteins collectively referred to as senescence associated secretory phenotype (SASP) (reviewed in ref.37). Therefore, the DEGs were analysed for the expression of genes whose encoded proteins are expected to be secreted, referred to as secretome. The secretome comprised 117/1005 (11.64%) of the DEGs in 9 months old *Myh6-Cre-Tmem43*$^{W/F}$ cardiac myocytes, the majority of which (86/117, 74%) was up-regulated. A heat map of differentially expressed secretome is presented in *Figure 6E*. Trophic and mitotic factors predicted to regulate expression of the differentially expressed secretome are presented in *Figure 6F*, which included AGT and TGFβ1 among the top regulators. A GSEA plot representing enrichment of genes involved in the SASP is shown in *Figure 6G*.[38]

To validate the findings, transcript levels of selected up- and down-regulated genes in the DDR pathway and SASP were analysed by RT-PCR in independent sets of samples. The results were largely concordant with those obtained by RNA-seq data (*Figure 6H* and Supplementary material online, *Figure S9*). Finally, to extend the findings, immunoblotting was performed to assess levels of selected secreted protein members of SASP, namely LGALS3, VCAN, and GDF15 (*Figure 6I*). Quantitative data showed increased levels of the selected SASP, which have a diverse array of functions, in the *Myh6-Cre-Tmem43*$^{W/F}$ hearts (*Figure 6J*).

3.11 Validation of TGFβ1-SMAD2/3 pathway activation

Given that TGFβ1 is the prototypic SASP protein and in view of enrichment of the TGFβ1 pathway targets, activation of EMT, and the prominence of myocardial fibrosis in the *Myh6-Cre-Tmem43*$^{W/F}$ hearts, the activation of the TGFβ1-SMAD2/3 pathway was further analysed by multiple complementary methods. To detect TGFβ1 expression in the heart, thin myocardial sections were stained with an anti TGFβ1 antibody followed by detection using a chromogenic DAB substrate. The data qualitatively suggested increased TGFβ1 expression in the *Myh6-*

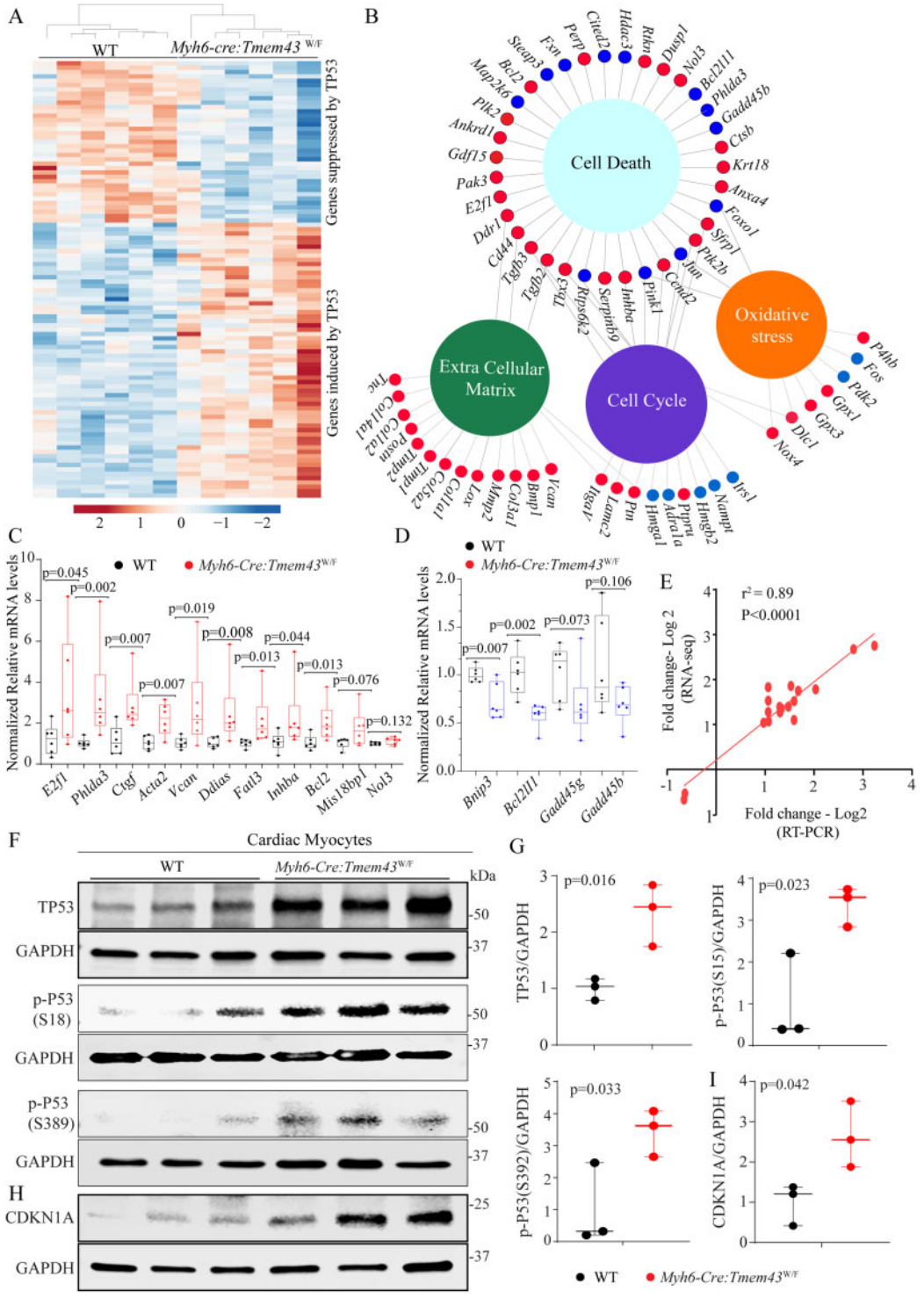

Figure 5 Validation of *TP53* activation in the *Myh6-Cre:Tmem43*$^{W/F}$ cardiac myocytes. (*A*) The heat map depicting altered transcript levels of the TP53 target genes in the *Myh6-Cre:Tmem43*$^{W/F}$ myocytes. Genes expected to be suppressed or activated upon activation of TP53 are shown. (*B*) Gene network (plotted using DiVenn application) for TP53 targets obtained from IPA demonstrating dysregulation of genes involved in four major biological functions associated with the TP53 pathway, namely, cell death, extracellular matrix, cell cycle, and oxidative stress. Red and blue nodes denote up-regulated and down regulated TP53 target genes in the network, respectively.(*C*–*E*) RT-PCR data showing transcript levels of 15 selected TP53 target genes, including those up-regulated (*C*) or down-regulated (*D*) in independent biological samples. (*E*) Panel depicts correlation in the transcript levels of selected TP53 target genes as analysed by RNA-Seq and RT-PCR techniques (N = 18, Pearson r^2 = 0.89). (*F* and *G*) Immunoblots and the quantitative data showing increased total, phospho (Ser18), and phosphor (Ser 389) TP53 protein levels in the *Myh6-Cre:Tmem43*$^{W/F}$ cardiac myocytes (N = 3; unpaired t-test P-values). (*H* and *I*) Immunoblots and the quantitative data showing increased CDKN1A protein levels, a bona fide target of the TP53 activation, in the *Myh6-Cre:Tmem43*$^{W/F}$ cardiac myocytes (N = 3; unpaired t-test P-values).

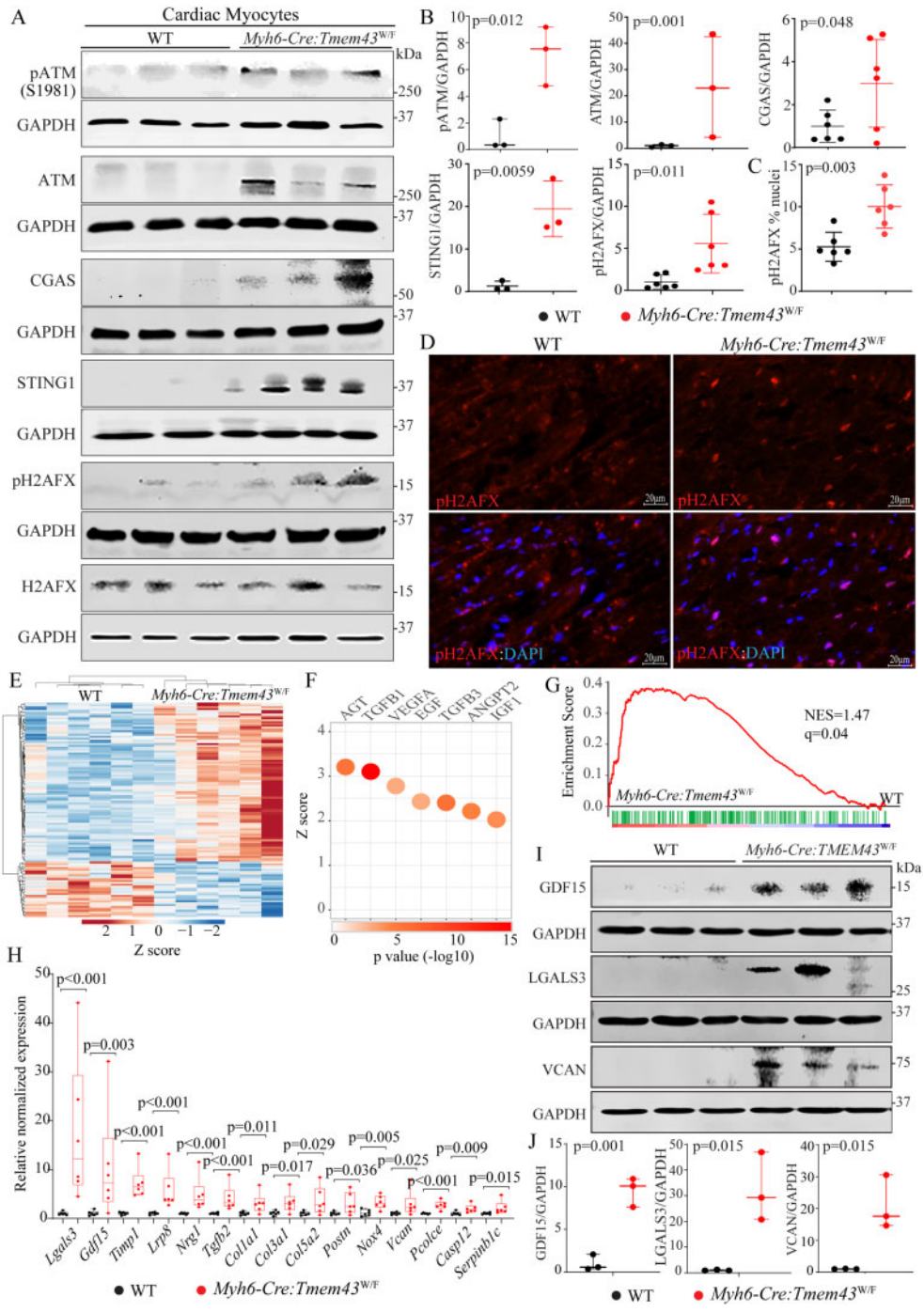

Figure 6 DNA damage response (DDR) and senescence associated secretary phenotype (SASP). (*A*) Immunoblots showing increased expression of several proteins in the DDR pathways, namely pATM, total ATM, CGAS, STING1, pH2AFX, and total H2AFX in the in the *Myh6-Cre:Tmem43*$^{W/F}$ myocytes. (*B*) Quantitative data representing protein levels of DNA damage markers. *N* = 3–6, *P*-values by unpaired *t*-test). (*C*) Graph depicting the percentage of nuclei stained positive for pH2AFX upon immunofluorescence staining of thin myocardial sections. Approximately, 20 000 nuclei per genotype were scored and percentage positive nuclei were compared between WT and *Myh6-Cre:Tmem43*$^{W/F}$ mice by *t*-test. (*D*) Immunofluorescence panels showing thin myocardial sections probed with an antibody against pH2AFX, a marker of double-stranded DNA breaks (DSBs). The number of nuclei expressing p2H2AFX was increased in the *Myh6-Cre:Tmem43*$^{W/F}$ myocytes, as shown in panel *C*. (*E*) Heat map of differentially expressed genes (DEGs) encoding secreted proteins (secretome) in *Myh6-Cre:Tmem43*$^{W/F}$ myocytes, as determined from the RNA-Seq data. (*F*) Top trophic and mitotic factors predicted to regulate expression of the secretome. (*G*) Gene set enrichment analysis (GSEA) showing enrichment of SASP in the *Myh6-Cre:Tmem43*$^{W/F}$ myocytes. Normalized enrichment score (NES) and the *q*-value are shown. (*H*) Reverse transcriptase-polymerase chain reaction (RT-PCR) of transcript levels of selected genes coding for secretome. Unpaired *t*-test *P*-values are depicted *N* = 6 per group). (*I*) Immunoblots showing expression of the selected secretome proteins in the *Myh6-Cre:Tmem43*$^{W/F}$ hearts. (*J*) Quantitative data showing increased GDF15, VCAN, and LGALS3, SASP markers, in the *Myh6-Cre:Tmem43*$^{W/F}$ hearts (*N* = 3 per group, unpaired *t*-test).

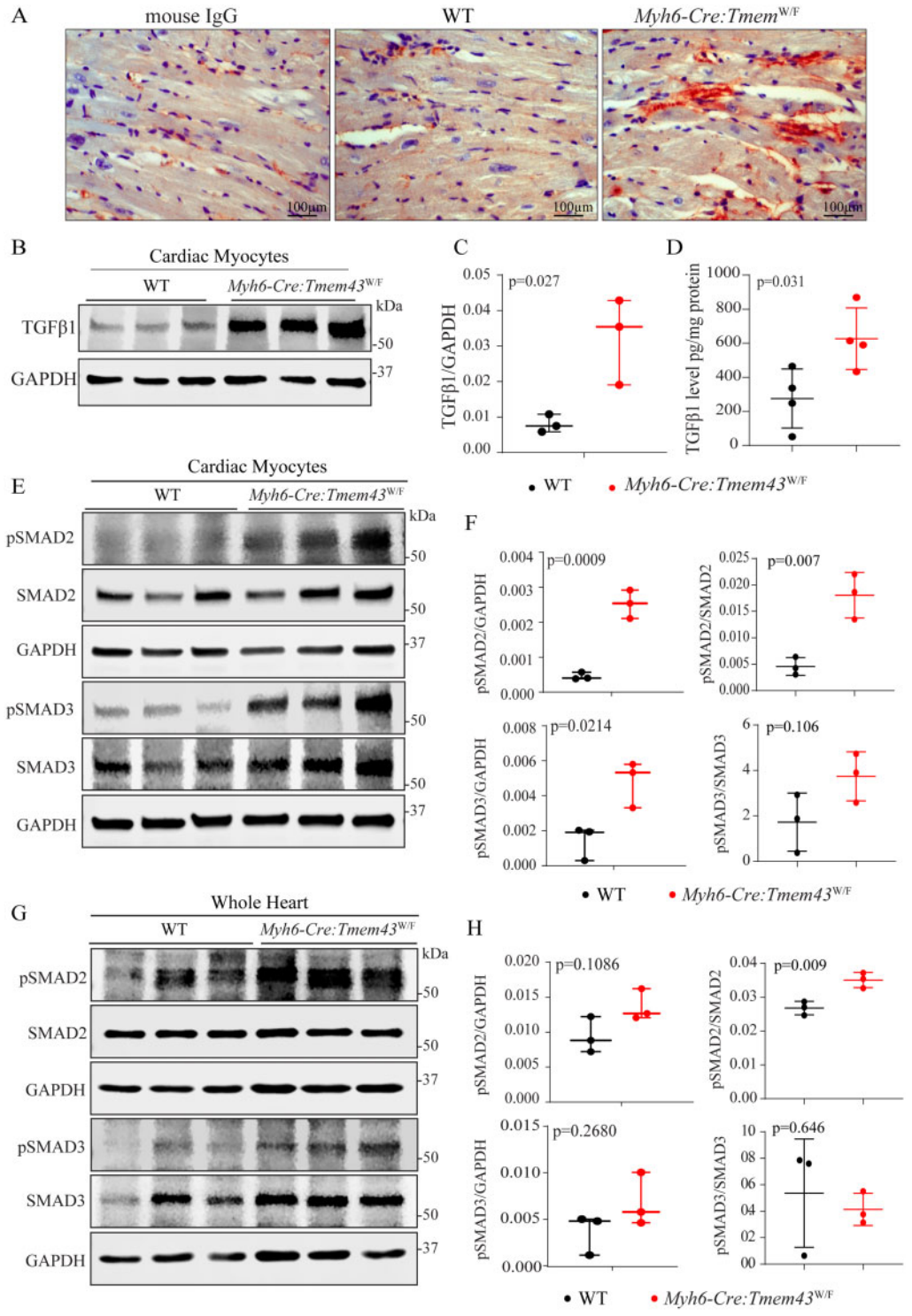

Figure 7 Activation of TGFβ1-SMAD2/3 l pathway in the *Myh6-Cre:Tmem43*$^{W/F}$ myocytes. (*A*) Immunohistochemistry staining of thin myocardial sections using an anti-TGFβ1 antibody, suggesting increased expression of TGFβ1 in the *Myh6-Cre:Tmem43*$^{W/F}$ mouse myocardium. (*B* and *C*) Immunoblots and the corresponding quantitative data showing increased total TGFβ1 protein level in the *Myh6-Cre:Tmem43*$^{W/F}$ cardiac myocyte extracts ($N = 3$, unpaired *t*-test *P*-value). (*D*) Active TGFβ1 levels as determined by an ELISA showing increased levels of active TGFβ1 in the *Myh6-Cre:Tmem43*$^{W/F}$ cardiac myocytes ($N = 4$; unpaired *t*-test *P*-value). (*E* and *F*) Immunoblots showing protein levels of total and phospho- SMAD2 and SMAD3 in the *Myh6-Cre:Tmem43*$^{W/F}$ cardiac myocyte protein extracts (*E*). Quantitative analysis of the immunoblots, normalized to GAPDH or total SMADs, are shown in panel *F*. (*G* and *H*) Immunoblots showing protein levels of total and phospho-SMAD2 and SMAD3 in the *Myh6-Cre:Tmem43*$^{W/F}$ whole heart protein extracts (*G*). Quantitative data, are shown in panel *H*, show a modest increase in SMAD3 levels in the whole heart ($N = 3$, *P*-values were calculated by unpaired *t*-test).

Cre:Tmem43$^{W/F}$ compared to the WT mouse hearts (*Figure 7A*). In support of the immunohistochemistry data, immunoblotting of cardiac myocyte protein extracts showed increased TGFβ1 protein levels in the *Myh6-Cre:Tmem43*$^{W/F}$ myocytes (*Figure 7B and C*). To further substantiate the histochemical findings, levels of active TGFβ1 were determined in cardiac myocyte protein extracts by ELISA. The latter showed increased levels of active TGFβ1 by ∼2-fold in the *Myh6-Cre:Tmem43*$^{W/F}$ as compared to WT cardiac myocytes (*Figure 7D*).

To investigate the downstream effectors of the activated TGFβ1, the DEGs were analysed for enrichment of the TRs using EGSEA, which identified SMADs, the intracellular signal transducers of the canonical TGFβ1 signalling pathway, as the top activated TRs (Supplementary material online, *Figure S10*). Given this finding and in view of the well-recognized phosphorylation of SMAD2 and SMAD3 upon binding of TGFβ1 to its cognate receptors, expression levels of total and phosphorylated (p)SMAD2 and pSMAD3 were determined by immunoblotting in cardiac myocyte as well as the whole heart protein lysates. Levels of pSMAD2 and pSMAD3 in cardiac myocyte protein extracts from *Myh6-Cre:Tmem43*$^{W/F}$ mice were markedly increased, as compared to WT myocytes, whereas levels of total SMAD2 were unchanged and those of total SMAD3 were increased (*Figure 7E and F*). Levels of pSMAD2 and pSMAD3 in the whole heart protein lysates from the *Myh6-Cre:Tmem43*$^{W/F}$ mice were also increased, albeit they were less pronounced as compared to their levels in the isolated myocytes (*Figure 7G and H*).

3.12 Interactions between TMEM43, TGFβ1, and LMNA

To investigate the mechanism(s) associated with activation of the DDR/TP53/TGFβ1 pathway in the *Myh6-Cre:Tmem43*$^{W/F}$ mouse hearts, Co-IP studies were performed on myocardial protein extracts to detect interactions between TMEM43 and TGFβ1. However, the assay failed to detect co-immunoprecipitation of TGFβ1 with an anti-TMEM43 antibody and conversely, co-immunoprecipitation of TMEM43 with an anti-TGFβ1 antibody (data not presented). Because LMNA has been reported to interact with TGFβ1, an indirect interaction between TMEM43 and TGFβ1 through LMNA was explored upon cross-linked IP.[39] The findings are notable for co-immunoprecipitation of LMNA with an anti-TMEM43 antibody (Supplementary material online, *Figure S11*). However, TGFβ1 was not detected in the precipitate.

3.13 PP2A activity

Because TMEM43 interacts with LMNA and LMNA has been reported to interact with PP2A, which might affect phosphorylation of SMADs in the *Myh6-Cre:Tmem43*$^{W/F}$ cardiac myocytes, PP2A activity was analysed by an ELISA. There was no difference in the PP2A activity in the WT and *Myh6-Cre:Tmem43*$^{W/F}$ cardiac myocytes (Supplementary material online, *Figure S12*).

4. Discussion

Cardiac myocyte-restricted heterozygous deletion of the *Tmem43* gene in mouse leads to activation of the DDR/TP53 pathways and expression of SASP, which is associated with a late-onset cardiomyopathy characterized by cardiac dilatation, systolic dysfunction, myocardial fibrosis, and apoptosis. The findings support the pathogenic role of *TMEM43* haploinsufficiency in human hereditary cardiomyopathy and provide novel mechanistic insights by implicating activation of the DDR/TP53 pathway as an underpinning mechanism.

The clinical and histological phenotype in the *Myh6-Cre:Tmem43*$^{W/F}$ mice are in accord with the molecular findings, including the cardiac myocyte RNA-seq data obtained at two-time points. Serial analysis of RNA-seq enabled identification of the early changes, which predicted activation of the TP53 pathway as a regulator of gene expression in the early stages of the disease. The approach also led to detection of the dysregulated pathways that occur in the context of cardiac phenotype, including the DDR pathway. The findings were concordant across multiple platforms and were verified by complementary methods. For example, activation of the TGFβ1-SMAD2-3 pathway, which was predicted based on the RNA-seq data, was verified by RT-PCR, immunoblotting, immunohistochemistry, and ELISA, all showing concordant findings.

The mechanism(s) of activation of the DDR pathway in the *Myh6-Cre:Tmem43*$^{W/F}$ myocytes was partially explored but remains unclear. Crossed-liked immunoprecipitation data indicated an interaction between TMEM43 and LMNA, as the latter is known to interact with the chromatin extensively and protect genomic DNA damage.[18,33] Mutations in the *LMNA* gene or *Lmna* haploinsufficiency are associated with activation of DDR, likely because of increased DSBs, and cascade activation of TP53 and related targets.[18,33] Thus, it is plausible that TMEM43 haploinsufficiency to induce DSBs and release of the genomic DNA into the cytosol through mechanisms similar to those involved in laminopathies or indirectly through interaction with LMNA. The cytosolic DNA is then sensed by CGAS, which targets STING1 and its downstream effectors, which were activated in the *Myh6-Cre:Tmem43*$^{W/F}$ myocytes. Consequently, activation of the TP53 and expression of SASP, including TGFβ1 are the consequences of activation of the DDR. SAPs target myocytes as well as non-myocyte cells in the myocardium, leading to cell senescence, impaired proliferation, apoptosis, and fibrosis. The exact nature of the DNA damage leading to activation of the DDR was not elucidated but presumably entails DSBs, based on changes in the molecular markers of DSBs, such as ATM and pH2AFX. There was also notable variability in the expression levels of molecular markers of DNA damage in the *Myh6-Cre:Tmem43*$^{W/F}$ mouse hearts, which was in accord with variability in the phenotypic expression of the disease in this mouse model. While technical reasons for the observed variability cannot be unambiguously excluded, its presence across multiple techniques and for multiple phenotypes suggests a biological basis. The basis for variability in the phenotypic expression of the disease is unclear. Finally, there were cell-type-specific differences in expression of genes involved in apoptosis and the apoptotic marker cleaved CASP3, which were increased in cardiac myocytes but not in cardiac fibroblasts. Similarly, differences in the transcript levels of selected genes differed between the myocytes and the whole myocardium, likely reflective of cellular heterogeneity of the latter.

Alternative mechanisms pertaining to activation of the TGFβ1 were also explored, including interactions between TGFβ1 and TMEM43 through Co-IP studies. Whereas a direct interaction was not detected, an indirect interaction through LMNA is speculated as the latter is known to interact with TGFβ1 as well as PP2A. However, PP2A activity was unchanged, excluding it as a mechanism for increased levels of pSMAD2/3. Given these findings, one might surmise that TGFβ1 activation, an archetypical SASP, was a consequence of TP53 activation, as the two pathways are well known to interact.[40–42] Considering the findings of the present study, interactions between TMEM43 and LMNA, and involvement of the LMNA and other nuclear envelop proteins in DNA damage and repair mechanisms, one might speculate that activation of

the DDR/TP53 and consequently, expression of SAPS, including TGFβ1, are common mechanisms in the pathogenesis of cardiomyopathies caused by mutations in genes encoding nuclear envelope proteins.[18,43]

Early activation of the TP53 pathway in the *Myh6-Cre:Tmem43*$^{W/F}$ myocytes was concurrent with induction of the pathways involved in protein synthesis, a finding that is consistent with the role of TP53 in cardiac myocyte hypertrophic remodelling.[44] This observation is also consistent with the established role of TP53 in regulating expression of a large number of cardiac genes, including those involved in maintaining cardiac structure and function.[45] Persistent activation of the TP53 pathway is, however, considered detrimental to cardiac structure and function, which is in accord with the findings of the present study.[18,46] Collectively, the data suggest the pathogenic role of the TP53 pathway in induction of the cardiac phenotype in the *Myh6-Cre:Tmem43*$^{W/F}$ mice.

The increased transcriptional activity of the TP53 in cardiac myocytes from 4 months old *Myh6-Cre:Tmem43*$^{W/F}$ mice, which was predicted based on the increased transcript levels of its target genes, was in accord with modest increases in the levels of phosphorylated TP53 proteins. The latter likely results in increased recruitment of the TP53 protein to the promoter regions. Increased promoter occupancy by TP53 might be an early marker of activation of DDR pathway, as levels of the CGAS, STING1, and pH2AFX proteins were unchanged at the early time point. However, at a later time point, not only levels of the TP53, including phospho-TP53 were markedly increased but also proteins levels of several markers of the DDR pathway, including pH2AFX, CGAS, and STING1 were increased. Activation of TP53 in the *Myh6-Cre:Tmem43*$^{W/F}$ myocytes was concordant with increased levels of phospho-ATM, suggesting activation in response to DSBs. The present data showing early activation of TP53 pathway in the *Myh6-Cre:Tmem43*$^{W/F}$ myocytes are in accord with the previous data showing its activation in the LMNA-related cardiomyopathy.[18] Taken together, one might speculate that activation of the DDR/TP53 pathway provides a shared mechanism for the pathogenesis of cardiomyopathy caused by deficiencies of these two nuclear inner membrane proteins. In addition, TP53 is also known to interact with SMADs, the downstream effectors of the TGFβ1, which provides a plausible mechanism for increased myocardial fibrosis in ACM caused by mutations in genes encoding nuclear envelope proteins.[42] In agreement with this notion, genetic deletion of the *Tp53* gene in mice attenuated myocardial fibrosis in a mouse model of laminopathies.[18]

The phenotype in the *Myh6-Cre:Tmem43*$^{W/F}$ mice had a late onset and was notable for a marked reduction in survival as well as LV dilatation and dysfunction. The findings in the *Myh6-Cre:Tmem43*$^{W/F}$ mice are in principle in agreement with the observed partial reduction in TMEM43 levels as well as the phenotype observed in a transgenic mouse model, over-expressing a mutant TMEM43 protein, namely p.Ser358Leu, associated with human ACM.[47] The phenotype in the *Myh6-Cre:Tmem43*$^{W/F}$ mice, however, was milder than the phenotype described in the TMEM43$^{p.Ser358Leu}$ transgenic mice, as reflected in a longer mean survival time, milder cardiac dysfunction, and lesser myocardial fibrosis.[47] Whereas the p.Ser358Leu is the most commonly described founder mutation in ACM, about a dozen frameshift and deletion variants in the *TMEM43* gene also have been reported in patients with ACM[16,17] (https://www.ncbi.nlm.nih.gov/clinvar). However, an unambiguous assignment of causality to variants leading to *TMEM43* haploinsufficiency has remained challenging because of the sporadic nature of the cases or the small size of the families, which suggests modest effect sizes of such variants. The findings of the present study suggest that haploinsufficiency of the *Tmem43* gene is sufficient to induce a relatively mild and late-onset phenotype, resembling ACM, as opposed to over-expression of the missense mutation, which induces early and severe phenotype in mice.[47] The findings are in contrast with those of a previous study reporting that deletion of *Tmem43* gene under the transcriptional regulation of the *Sox2* promoter did not induce a discernible phenotype at rest or in response to stressors.[48] The reason(s) for the observed differences between the mouse models of *Tmem43* haploinsufficiency might reflect differences in the experimental design, such as the use of the *Sox2* promoter, which is active during development in most cell types as opposed to the use of *Myh6* promoter, which is active in adult cardiac myocytes. In addition, Cre-mediated recombination efficiency regulated by *Sox2* and *Myh6* promoters might differ and account for the disparity in the phenotype in the mouse models. Finally, long-term expression of Cre recombinase under transcriptional activity of the *Myh6* promoter as opposed to its transient expression under the *Sox2* promoter might provide an additional impetus for the induction of the phenotype in the *Myh6-Cre:Tmem43*$^{W/F}$ mice. Nevertheless, the *Myh6-Cre* mice alone were included in the phenotypic characterization and did not exhibit a discernible phenotype.

In conclusion, haploinsufficiency of the *Tmem43* gene specifically in cardiac myocytes leads to a late-onset cardiomyopathy characterized by myocardial fibrosis and apoptosis, likely mediated by activation of the DDR/TP53 pathway. The findings implicate the DDR/TP53/TGFβ1 pathway as a common pathway in the pathogenesis of cardiomyopathies caused by mutations in genes encoding nuclear membrane proteins and identify it as a potential therapeutic target in this subset of heart failure.

Supplementary material

Supplementary material is available at *Cardiovascular Research* online.

Authors' contributions

L.R. performed the vast majority of the experiments. S.M.C. performed some of the western blotting, immunofluorescent, and co-immunoprecipitation studies. S.F. performed some of the western blotting experiments. S.N.C. performed the initial phenotypic characterization of the mice, including initial western blotting. R.L. analysed the initial echocardiographic data. X.C. established the mouse lines and contributed to initial analysis of the phenotype. C.C. and M.J.R. performed the bioinformatics analysis of the RNA-sequencing data. P.G. performed secondary bioinformatics analysis of RNA-Sequencing data, contributed to data analysis and edited the manuscript. A.J.M. conceived the studies, supervised the experiments and wrote the manuscript.

Conflict of interest: none declared.

Funding

This work was supported in part by grants from NIH, National Heart, Lung and Blood Institute (NHLBI R01 HL132401, R01 HL151737, and S10 OD018135), Leducq Foundation (14 CVD 03), NIA (R21 AG060413-01), the Ewing Halsell Foundation, George and Mary Josephine Hamman Foundation, TexGen Fund from Greater Houston Community Foundation.

References

1. Corrado D, Basso C, Judge DP. Arrhythmogenic cardiomyopathy. *Circ Res* 2017;**121**: 784–802.
2. Corrado D, Link MS, Calkins H. Arrhythmogenic right ventricular cardiomyopathy. *N Engl J Med* 2017;**376**:61–72.
3. Marian AJ, Asatryan B, Wehrens XHT. Genetic basis and molecular biology of cardiac arrhythmias in cardiomyopathies. *Cardiovasc Res* 2020;**116**:1600–1619.
4. Marcus FI, Fontaine GH, Guiraudon G, Frank R, Laurenceau JL, Malergue C, Grosgogeat Y. Right ventricular dysplasia: a report of 24 adult cases. *Circulation* 1982; **65**:384–398.
5. Basso C, Thiene G, Corrado D, Angelini A, Nava A, Valente M. Arrhythmogenic right ventricular cardiomyopathy. Dysplasia, dystrophy, or myocarditis? *Circulation* 1996;**94**: 983–991.
6. Broussard JA, Getsios S, Green KJ. Desmosome regulation and signaling in disease. *Cell Tissue Res* 2015;**360**:501–512.
7. Manring HR, Dorn LE, Ex-Willey A, Accornero F, Ackermann MA. At the heart of inter- and intracellular signaling: the intercalated disc. *Biophys Rev* 2018;**10**:961–971.
8. Garcia-Gras E, Lombardi R, Giocondo MJ, Willerson JT, Schneider MD, Khoury DS, Marian AJ. Suppression of canonical Wnt/beta-catenin signaling by nuclear plakoglobin recapitulates phenotype of arrhythmogenic right ventricular cardiomyopathy. *J Clin Invest* 2006;**116**:2012–2021.
9. Chen SN, Gurha P, Lombardi R, Ruggiero A, Willerson JT, Marian AJ. The hippo pathway is activated and is a causal mechanism for adipogenesis in arrhythmogenic cardiomyopathy. *Circ Res* 2014;**114**:454–468.
10. Mayosi BM, Fish M, Shaboodien G, Mastantuono E, Kraus S, Wieland T, Kotta MC, Chin A, Laing N, Ntusi NB, Chong M, Horsfall C, Pimstone SN, Gentilini D, Parati G, Strom TM, Meitinger T, Pare G, Schwartz PJ, Crotti L. Identification of cadherin 2 (CDH2) mutations in arrhythmogenic right ventricular cardiomyopathy. *Circ Cardiovasc Genet* 2017;**10**:e001605.
11. van Hengel J, Calore M, Bauce B, Dazzo E, Mazzotti E, De Bortoli M, Lorenzon A, Li Mura IE, Beffagna G, Rigato I, Vleeschouwers M, Tyberghein K, Hulpiau P, van Hamme E, Zaglia T, Corrado D, Basso C, Thiene G, Daliento L, Nava A, van Roy F, Rampazzo A. Mutations in the area composita protein alphaT-catenin are associated with arrhythmogenic right ventricular cardiomyopathy. *Eur Heart J* 2013;**34**:201–210.
12. Ortiz-Genga MF, Cuenca S, Dal Ferro M, Zorio E, Salgado-Aranda R, Climent V, Padrón-Barthe L, Duro-Aguado I, Jiménez-Jáimez J, Hidalgo-Olivares VM, García-Campo E, Lanzillo C, Suárez-Mier MP, Yonath H, Marcos-Alonso S, Ochoa JP, Santomé JL, García-Giustiniani D, Rodríguez-Garrido JL, Domínguez F, Merlo M, Palomino J, Peña ML, Trujillo JP, Martín-Vila A, Stolfo D, Molina P, Lara-Pezzi E, Calvo-Iglesias FE, Nof E, Calò L, Barriales-Villa R, Gimeno-Blanes JR, Arad M, García-Pavía P, Monserrat L. Truncating FLNC mutations are associated with high-risk dilated and arrhythmogenic cardiomyopathies. *J Am Coll Cardiol* 2016;**68**:2440–2451.
13. van der Zwaag PA, van Rijsingen IA, Asimaki A, Jongbloed JD, van Veldhuisen DJ, Wiesfeld AC, Cox MG, van Lochem LT, de Boer RA, Hofstra RM, Christiaans I, van Spaendonck-Zwarts KY, Lekanne dit Deprez RH, Judge DP, Calkins H, Suurmeijer AJ, Hauer RN, Saffitz JE, Wilde AA, van den Berg MP, van Tintelen JP. Phospholamban R14del mutation in patients diagnosed with dilated cardiomyopathy or arrhythmogenic right ventricular cardiomyopathy: evidence supporting the concept of arrhythmogenic cardiomyopathy. *Eur J Heart Fail* 2012;**14**:1199–1207.
14. Parikh VN, Caleshu C, Reuter C, Lazzeroni LC, Ingles J, Garcia J, McCaleb K, Adesiyun T, Sedaghat-Hamedani F, Kumar S, Graw S, Gigli M, Stolfo D, Dal Ferro M, Ing AY, Nussbaum R, Funke B, Wheeler MT, Hershberger RE, Cook S, Steinmetz LM, Lakdawala NK, Taylor MRG, Mestroni L, Merlo M, Sinagra G, Semsarian C, Meder B, Judge DP, Ashley E. Regional variation in RBM20 causes a highly penetrant arrhythmogenic cardiomyopathy. *Circ Heart Fail* 2019;**12**:e005371.
15. Quarta G, Syrris P, Ashworth M, Jenkins S, Zuborne Alapi K, Morgan J, Muir A, Pantazis A, McKenna WJ, Elliott PM. Mutations in the Lamin A/C gene mimic arrhythmogenic right ventricular cardiomyopathy. *Eur Heart J* 2012;**33**:1128–1136.
16. Merner ND, Hodgkinson KA, Haywood AF, Connors S, French VM, Drenckhahn JD, Kupprion C, Ramadanova K, Thierfelder L, McKenna W, Gallagher B, Morris-Larkin L, Bassett AS, Parfrey PS, Young TL. Arrhythmogenic right ventricular cardiomyopathy type 5 is a fully penetrant, lethal arrhythmic disorder caused by a missense mutation in the TMEM43 gene. *Am J Hum Genet* 2008;**82**:809–821.
17. Dominguez F, Zorio E, Jimenez-Jaimez J, Salguero-Bodes R, Zwart R, Gonzalez-Lopez E, Molina P, Bermúdez-Jiménez F, Delgado JF, Braza-Boïls A, Bornstein B, Toquero J, Segovia J, Van Tintelen JP, Lara-Pezzi E, Garcia-Pavia P. Clinical characteristics and determinants of the phenotype in TMEM43 arrhythmogenic right ventricular cardiomyopathy type 5. *Heart Rhythm* 2020;**17**:945–954.
18. Chen SN, Lombardi R, Karmouch J, Tsai JY, Czernuszewicz G, Taylor MRG, Mestroni L, Coarfa C, Gurha P, Marian AJ. DNA damage response/TP53 pathway is activated and contributes to the pathogenesis of dilated cardiomyopathy associated with LMNA (Lamin A/C) mutations. *Circ Res* 2019;**124**:856–873.
19. Cheedipudi SM, Hu J, Fan S, Yuan P, Karmouch J, Czernuszewicz G, Robertson MJ, Coarfa C, Hong K, Yao Y, Moore HC, Wehrens X, Gurha P, Marian AJ. Exercise restores dysregulated gene expression in a mouse model of arrhythmogenic cardiomyopathy. *Cardiovasc Res* 2020;**116**:1199–1213.
20. Auguste G, Gurha P, Lombardi R, Coarfa C, Willerson JT, Marian AJ. Suppression of activated FOXO transcription factors in the heart prolongs survival in a mouse model of laminopathies. *Circ Res* 2018;**122**:678–692.
21. Karmouch J, Zhou QQ, Miyake CY, Lombardi R, Kretzschmar K, Bannier-Helaouet M, Clevers H, Wehrens XHT, Willerson JT, Marian AJ. Distinct cellular basis for early cardiac arrhythmias, the cardinal manifestation of arrhythmogenic cardiomyopathy, and the skin phenotype of cardiocutaneous syndromes. *Circ Res* 2017;**121**: 1346–1359.
22. Chen SN, Czernuszewicz G, Tan Y, Lombardi R, Jin J, Willerson JT, Marian AJ. Human molecular genetic and functional studies identify TRIM63, encoding Muscle RING Finger Protein 1, as a novel gene for human hypertrophic cardiomyopathy. *Circ Res* 2012;**111**:907–919.
23. Ruggiero A, Chen SN, Lombardi R, Rodriguez G, Marian AJ. Pathogenesis of hypertrophic cardiomyopathy caused by myozenin 2 mutations is independent of calcineurin activity. *Cardiovasc Res* 2013;**97**:44–54.
24. Bergmann O, Jovinge S. Isolation of cardiomyocyte nuclei from post-mortem tissue. *J Vis Exp* 2012;**65**:4205.
25. Bergmann O, Zdunek S, Alkass K, Druid H, Bernard S, Frisen J. Identification of cardiomyocyte nuclei and assessment of ploidy for the analysis of cell turnover. *Exp Cell Res* 2011;**317**:188–194.
26. O'Connell TD, Rodrigo MC, Simpson PC. Isolation and culture of adult mouse cardiac myocytes. *Methods Mol Biol* 2007;**357**:271–296.
27. Kim D, Paggi JM, Park C, Bennett C, Salzberg SL. Graph-based genome alignment and genotyping with HISAT2 and HISAT-genotype. *Nat Biotechnol* 2019;**37**: 907–915.
28. Liao Y, Smyth GK, Shi W. featureCounts: an efficient general purpose program for assigning sequence reads to genomic features. *Bioinformatics* 2014;**30**: 923–930.
29. Love MI, Huber W, Anders S. Moderated estimation of fold change and dispersion for RNA-seq data with DESeq2. *Genome Biol* 2014;**15**:550.
30. Hochberg Y, Benjamini Y. More powerful procedures for multiple significance testing. *Stat Med* 1990;**9**:811–818.
31. Alhamdoosh M, Ng M, Wilson NJ, Sheridan JM, Huynh H, Wilson MJ, Ritchie ME. Combining multiple tools outperforms individual methods in gene set enrichment analyses. *Bioinformatics* 2017;**33**:414–424.
32. Lombardi R, da Graca Cabreira-Hansen M, Bell A, Fromm RR, Willerson JT, Marian AJ. Nuclear plakoglobin is essential for differentiation of cardiac progenitor cells to adipocytes in arrhythmogenic right ventricular cardiomyopathy. *Circ Res* 2011;**109**: 1342–1353.
33. Cheedipudi SM, Matkovich SJ, Coarfa C, Hu X, Robertson MJ, Sweet M, Taylor M, Mestroni L, Cleveland J, Willerson JT, Gurha P, Marian AJ. Genomic reorganization of lamin-associated domains in cardiac myocytes is associated with differential gene expression and DNA methylation in human dilated cardiomyopathy. *Circ Res* 2019; **124**:1198–1213.
34. Preissl S, Schwaderer M, Raulf A, Hesse M, Gruning BA, Kobele C, Backofen R, Fleischmann BK, Hein L, Gilsbach R. Deciphering the epigenetic code of cardiac myocyte transcription. *Circ Res* 2015;**117**:413–423.
35. Krenning L, van den Berg J, Medema RH. Life or death after a break: what determines the choice? *Mol Cell* 2019;**76**:346–358.
36. Blackford AN, Jackson SP. ATM, ATR, and DNA-PK: the trinity at the heart of the DNA damage response. *Mol Cell* 2017;**66**:801–817.
37. Lecot P, Alimirah F, Desprez PY, Campisi J, Wiley C. Context-dependent effects of cellular senescence in cancer development. *Br J Cancer* 2016;**114**:1180–1184.
38. Basisty N, Kale A, Jeon OH, Kuehnemann C, Payne T, Rao C, Holtz A, Shah S, Sharma V, Ferrucci L, Campisi J, Schilling B. A proteomic atlas of senescence-associated secretomes for aging biomarker development. *PLoS Biol* 2020;**18**: e3000599.
39. Van Berlo JH, Voncken JW, Kubben N, Broers JL, Duisters R, van Leeuwen RE, Crijns HJ, Ramaekers FC, Hutchison CJ, Pinto YM. A-type lamins are essential for TGF-beta1 induced PP2A to dephosphorylate transcription factors. *Hum Mol Genet* 2005;**14**:2839–2849.
40. Cordenonsi M, Dupont S, Maretto S, Insinga A, Imbriano C, Piccolo S. Links between tumor suppressors: p53 is required for TGF-beta gene responses by cooperating with Smads. *Cell* 2003;**113**:301–314.
41. Dupont S, Zacchigna L, Adorno M, Soligo S, Volpin D, Piccolo S, Cordenonsi M. Convergence of p53 and TGF-beta signaling networks. *Cancer Lett* 2004;**213**: 129–138.
42. Wilkinson DS, Ogden SK, Stratton SA, Piechan JL, Nguyen TT, Smulian GA, Barton MC. A direct intersection between p53 and transforming growth factor beta pathways targets chromatin modification and transcription repression of the alpha-fetoprotein gene. *MCB* 2005;**25**:1200–1212.
43. Moser B, Basilio J, Gotzmann J, Brachner A, Foisner R. Comparative interactome analysis of Emerin, MAN1 and LEM2 reveals a unique role for LEM2 in nucleotide excision repair. *Cells* 2020;**9**:463.
44. Nomura S, Satoh M, Fujita T, Higo T, Sumida T, Ko T, Yamaguchi T, Tobita T, Naito AT, Ito M, Fujita K, Harada M, Toko H, Kobayashi Y, Ito K, Takimoto E, Akazawa H,

Morita H, Aburatani H, Komuro I. Cardiomyocyte gene programs encoding morphological and functional signatures in cardiac hypertrophy and failure. *Nat Commun* 2018;**9**:4435.
45. Mak TW, Hauck L, Grothe D, Billia F. p53 regulates the cardiac transcriptome. *Proc Natl Acad Sci USA* 2017;**114**:2331–2336.
46. Sano M, Minamino T, Toko H, Miyauchi H, Orimo M, Qin Y, Akazawa H, Tateno K, Kayama Y, Harada M, Shimizu I, Asahara T, Hamada H, Tomita S, Molkentin JD, Zou Y, Komuro I. p53-induced inhibition of Hif-1 causes cardiac dysfunction during pressure overload. *Nature* 2007;**446**:444–448.
47. Padrón-Barthe L, Villalba-Orero M, Gómez-Salinero JM, Domínguez F, Román M, Larrasa-Alonso J, Ortiz-Sánchez P, Martínez F, López-Olañeta M, Bonzón-Kulichenko E, Vázquez J, Martí-Gómez C, Santiago DJ, Prados B, Giovinazzo G, Gómez-Gaviro MV, Priori S, Garcia-Pavia P, Lara-Pezzi E. Severe cardiac dysfunction and death caused by arrhythmogenic right ventricular cardiomyopathy type 5 are improved by inhibition of glycogen synthase kinase-3beta. *Circulation* 2019;**140**:1188–1204.
48. Stroud MJ, Fang X, Zhang J, Guimaraes-Camboa N, Veevers J, Dalton ND, Gu Y, Bradford WH, Peterson KL, Evans SM, Gerace L, Chen J. Luma is not essential for murine cardiac development and function. *Cardiovasc Res* 2018;**114**:378–388.

Translational perspective

The data indicate that the DNA damage response (DDR) to double stranded DNA breaks (DSBs) is activated in a mouse model of cardiomyopathy caused by haploinsufficiency of the *Tmem43* gene. The *TMEM43* gene is a known cause of arrhythmogenic cardiomyopathy in humans. The DDR activates the TP53 pathway and leads to expression of senescence associated secretary phenotype (SASP), such as TGFβ1, which induce a senescence-associated pro-fibrotic cardiomyopathy.

These findings along with our previous data identify the DDR as a putative common mechanism in the pathogenesis of cardiomyopathies, and likely in the pathogenesis of over two dozen diseases, caused by mutations in the nuclear envelope proteins (envelopathies).

Erratum

doi:10.1093/cvr/cvab224
Online publish-ahead-of-print 16 July 2021

Erratum to: Hypertension, the renin–angiotensin system, and the risk of lower respiratory tract infections and lung injury: implications for COVID-19: European Society of Hypertension COVID-19 Task Force Review of Evidence

Reinhold Kreutz, Engi Abd El-Hady Algharably, Michel Azizi, Piotr Dobrowolski, Tomasz Guzik, Andrzej Januszewicz, Alexandre Persu, Aleksander Prejbisz, Thomas Günther Riemer, Ji-Guang Wang, Michel Burnier

Cardiovascular Research, Volume 116, Issue 10, 1 August 2020, Pages 1688–1699, https://doi.org/10.1093/cvr/cvaa097

In the originally published version of this manuscript, the following statement should have been included below the affiliations: "This paper was handled by Reviews Associate Editor, Ali J. Marian." This has now been corrected online. The publisher apologizes for the error.